Application of the Finite Element Method to Slope Stability

Rocscience Inc.
Toronto, 2001-2004

This document outlines the capabilities of the finite element method in the analysis of slope stability problems. The manuscript describes the constitutive laws of material behaviour such as the Mohr-Coulomb failure criterion, and material properties input parameters, required to adequately model slope failure. It also discusses advanced topics such as strength reduction techniques and the definition of slope collapse. Several slopes are analyzed with the finite element method, and the results compared with outcomes from various limit equilibrium methods. Conclusions for the practical use of the finite element method are also given.

1. Introduction

Slope stability analysis is an important area in geotechnical engineering. Most textbooks on soil mechanics include several methods of slope stability analysis. A detailed review of equilibrium methods of slope stability analysis is presented by Duncan (Duncan, 1996). These methods include the ordinary method of slices, Bishop's modified method, force equilibrium methods, Janbu's generalized procedure of Slices, Morgenstern and Price's method and Spencer's method. These methods, in general, require the soil mass to be divided into slices. The directions of the forces acting on each slice in the slope are assumed. This assumption is a key role in distinguishing one limit equilibrium method from another.

Limit equilibrium methods require a continuous surface passes the soil mass. This surface is essential in calculating the minimum factor of safety (FOS) against sliding or shear failure. Before the calculation of slope stability in these methods, some assumptions, for example, the side forces and their directions, have to be given out artificially in order to build the equations of equilibrium.

With the development of cheaper personal computer, finite element method has been increasingly used in slope stability analysis. The advantage of a finite element approach in the analysis of slope stability problems over traditional limit equilibrium methods is that no

assumption needs to be made in advance about the shape or location of the failure surface, slice side forces and their directions. The method can be applied with complex slope configurations and soil deposits in two or three dimensions to model virtually all types of mechanisms. General soil material models that include Mohr-Coulomb and numerous others can be employed. The equilibrium stresses, strains, and the associated shear strengths in the soil mass can be computed very accurately. The critical failure mechanism developed can be extremely general and need not be simple circular or logarithmic spiral arcs. The method can be extended to account for seepage induced failures, brittle soil behaviors, random field soil properties, and engineering interventions such as geo-textiles, soil nailing, drains and retaining walls (Swan et al, 1999). This method can give information about the deformations at working stress levels and is able to monitor progressive failure including overall shear failure (Griffiths, 1999).

Generally, there are two approaches to analyze slope stability using finite element method. One approach is to increase the gravity load and the second approach is to reduce the strength characteristics of the soil mass.

Phase^2 has been widely used in geotechnical and mining engineering as a tool for the design and the analysis of tunnel, surface excavation and ore extraction and supports (*Phase*^{2}, 1999). However, few applications have been reported in the area of slope stability analysis. Obviously, its potential applications in the most of areas in geotechnical engineering will be shown with time passing and the accumulation of users' experience.

This manuscript is prepared to validate the applicability of using the finite element program *Phase*^{2}, in the analysis of slope stability problems. Four slope stability examples are presented and compared to previous FEM work and limit equilibrium methods (Griffiths, 1999 and *Slide*)

2. Important aspects in slope stability analysis

In this section, three major aspects that influence slope stability analysis are discussed. The first is about the material properties of the slope model. The second is the influence of calculating factor of safety to slope stability and the third aspect is the definition of the slope failure.

i) Model material properties

This work applied only for two-dimensional plain-strain problems. The Mohr-Coulomb constitutive model used to describe the soil (or rock) material properties. The Mohr-Coulomb criterion relates the shear strength of the material to the cohesion, normal stress and angle of internal friction of the material. The failure surface of the Mohr-Coulomb model can be presented as:

$$f = \frac{I_1}{3}\sin\phi + \sqrt{J_2}\left[\cos\Theta - \frac{1}{3}\sin\Theta\sin\phi\right] - C\cos\phi \tag{1}$$

where ϕ is the angle of internal friction, C is cohesion and

$$I_1 = (\sigma_1 + \sigma_2 + \sigma_3) = 3\sigma_m \tag{2}$$

$$J_2 = \left(\frac{1}{2}\left(s_x^2 + s_y^2 + s_z^2\right) + \tau_{xy}^2 + \tau_{yz}^2 + \tau_{zx}^2\right) \tag{3}$$

$$\Theta = \frac{1}{3}\sin^{-1}\left[\frac{3\sqrt{3}J_3}{2J_2^{3/2}}\right] \tag{4}$$

where $J_3 = s_x s_y s_z + 2\tau_{xy}\tau_{yz}\tau_{zx} - s_x\tau_{yz}^2 - s_y\tau_{xz}^2 - s_z\tau_{xy}^2$
and $s_x = \sigma_x - \sigma_m$, $s_y = \sigma_y - \sigma_m$, $s_z = \sigma_z - \sigma_m$

For Mohr-Coulomb material model, six material properties are required. These properties are the friction angle ϕ, cohesion C, dilation angle ψ, Young's modulus E, Poisson's ratio ν and unit weight of soil γ. Young's modulus and Poisson's ratio have a profound influence on the computed deformations prior to slope failure, but they have little influence on the predicted factor of safety in slope stability analysis. Thus in this work two constant values for these parameters are used throughout the examples (E = 10^5 kN/m^2 and ν = 0.3).

Dilation angle, ψ affects directly the volume change during soil yielding. If $\psi = \phi$, the plasticity flow rule is known as "associated", and if $\psi \neq \phi$, the plasticity flow rule is considered as "no-associated". The change in the volume during the failure is not considered in this study and therefore the dilation angle is taken as 0. Therefore, only three parameters (friction angle, cohesion and unit weight of material) of the model material are considered in the modeling of slope failure.

ii) Factor of Safety (*FOS*) and Strength Reduction Factor (*SRF*).

Slope fails because of its material shear strength on the sliding surface is insufficient to resist the actual shear stresses. Factor of safety is a value that is used to examine the stability state of slopes. For *FOS* values greater than 1 means the slope is stable, while values lower that 1 means slope is instable. In accordance to the shear failure, the factor of safety against slope failure is simply calculated as:

$$FOS = \frac{\tau}{\tau_f} \tag{5}$$

Where τ is the shear strength of the slope material, which is calculated through Mohr-Coulomb criterion as:

$$\tau = C + \sigma_n \tan\phi \tag{6}$$

and τ_f is the shear stress on the sliding surface. It can be calculated as:

$$\tau_f = C_f + \sigma_n \tan\phi_f \tag{7}$$

where the factored shear strength parameters C_f and ϕ_f are:

$$C_f = \frac{C}{SRF} \tag{8}$$

$$\phi_F = \tan^{-1}\left(\frac{\tan\phi}{SRF}\right) \tag{9}$$

Where *SRF* is strength reduction factor. This method has been referred to as the 'shear strength reduction method'. To achieve the correct *SRF*, it is essential to trace the value of *FOS* that will just cause the slope to fail.

iii) Slope Collapse

Non-convergence within a user-specified number of iteration in finite element program is taken as a suitable indicator of slope failure. This actually means that no stress distribution can be achieved to satisfy both the Mohr-Coulomb criterion and global equilibrium. Slope failure and numerical non-convergence take place at the same time and are joined by an increase in the

displacements. Usually, value of the maximum nodal displacement just after slope failure has a big jump compared to the one before failure.

3. Slope stability benchmark example

To assess the accuracy of the proposed algorithm using *Phase*^{2}, simulations were performed for some specific parameters. The studied parameters include finite element type, maximum number of iterations and convergence factor, and the searching method for SRF.

The benchmark example considers a homogenous slope without foundation. The geometry of the slope is presented in Figure 1.

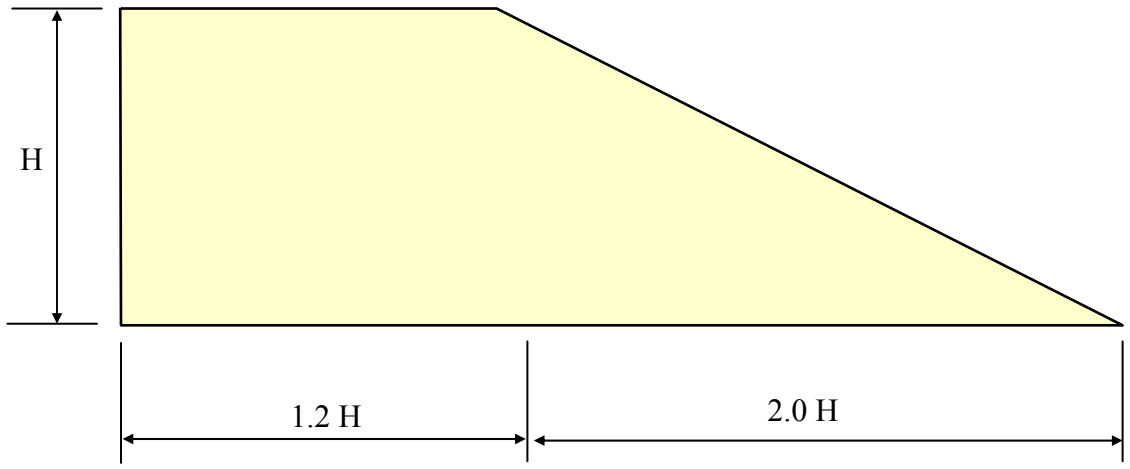

Figure 1. Model geometry

Gravity load is applied to the model and the strength reduction factor (*SRF*) gradually increased affecting equations (8) and (9) until convergence could not be achieved. The material parameters of the slope are given in Table 1.

Table1. Material properties

E (kN/m^2)	ν	γ (kN/m^3)	ϕ (degree)	C (kN/m^2)
100000	0.3	20	20	10

The first parameter studied in this example is the effect of different element types to the accuracy of the results *Phase*^{2} comes with four element types: 3 nodded triangle (T3), 6 nodded triangle (T6), 4 nodded quadrilateral (Q4) and 8 nodded quadrilateral (Q8). Two different meshes are used to discretize the slope geometry. The first mesh uses 1408 triangular elements. The second mesh is discretized with 104 elements. Results of the factor of safety for different element types are presented with comparison to Bishop's method and Griffith's FE result in Table 2.

Table 2. Factor of safety using different element types

Bishop	Griffiths	*Phase*^{2}			
		T3	T6	Q4	Q8
1.38	1.4	1.51	1.39	1.47	1.42

From table 2, the differences of the factor of safety using T3 and Q4 are larger than 5%, while the factors of safety using T6 and Q8 are close to Griffiths' and Bishop's results. Hence T6 and Q8 are used for the verification examples presented in the following sections.

The second parameter studied in this section is the effect of tolerance and number of iteration on the factor of safety. *Phase*^{2} uses a default value of 500 to the maximum number of iteration and a default value of 0.001 for the tolerance. Two values of maximum number of iteration are considered, 500 and 1000. Results from both cases were very close. For tolerance value, couple of values is assumed and the tolerance of 0.005 is chosen as an indicator.

The third parameter is the searching procedure. In this work, the procedure used to determine the strength reduction factor is

$$SRF_n = SRF_{n-1} \pm \frac{\left|SRF_{n-2} - SRF_{n-1}\right|}{2} \tag{9}$$

Equation (9) determines whether to increase or decrease the value of *SRF* in the next *FOS*.

4. Examples of slope stability analysis

As it is indicated in the previous section, two meshes will be considered in all the examples in this section. These meshes use T6 and Q8 elements.

Example 1. Homogeneous Slope with a Foundation Layer.

This problem is taken from the verification manual of *Slide* 3.0 (verification #1). Without considering pore water pressure, there is a homogeneous slope with a foundation layer. The slope model geometry is presented in Figure 2. The slope material properties are shown in table 3.

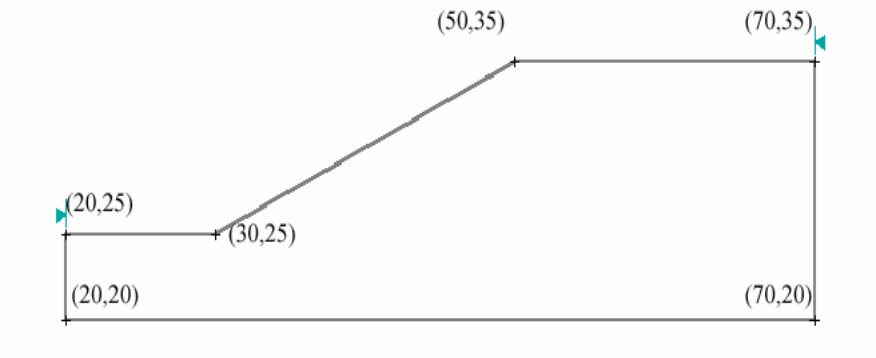

Figure 2. Slope model geometry

Table 3. Slope material properties

E (kN/m^2)	ν	γ (kN/m^3)	ϕ (degree)	C (kN/m^2)
100000	0.3	20.2	19.6	3.0

Figure 3 shows the two meshes used in this slope stability analysis. First mesh was discretized with 1515 T6 elements, while the second mesh was discretized with 104 Q8 elements. Vertical

rollers are used on the left and the right side of the geometry boundaries and full fixity at the bottoms of the geometry.

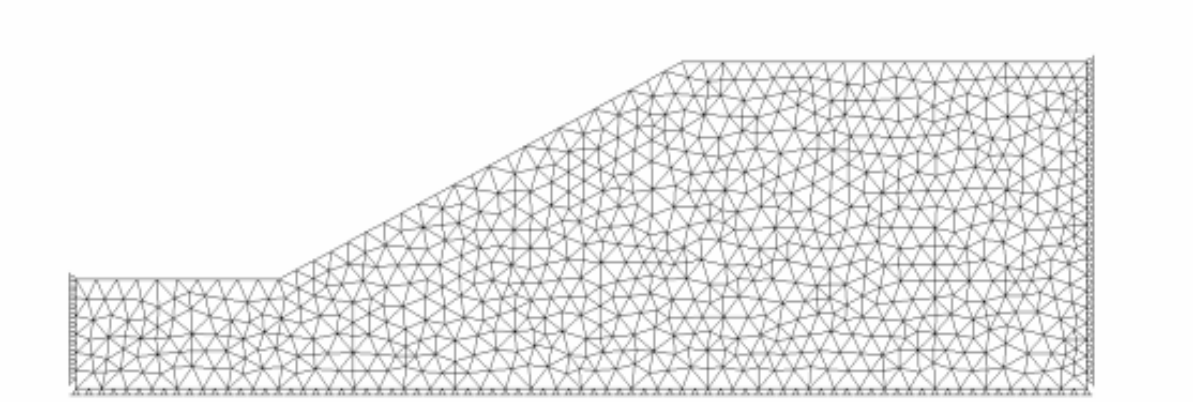

(a) Mesh with T6 elements

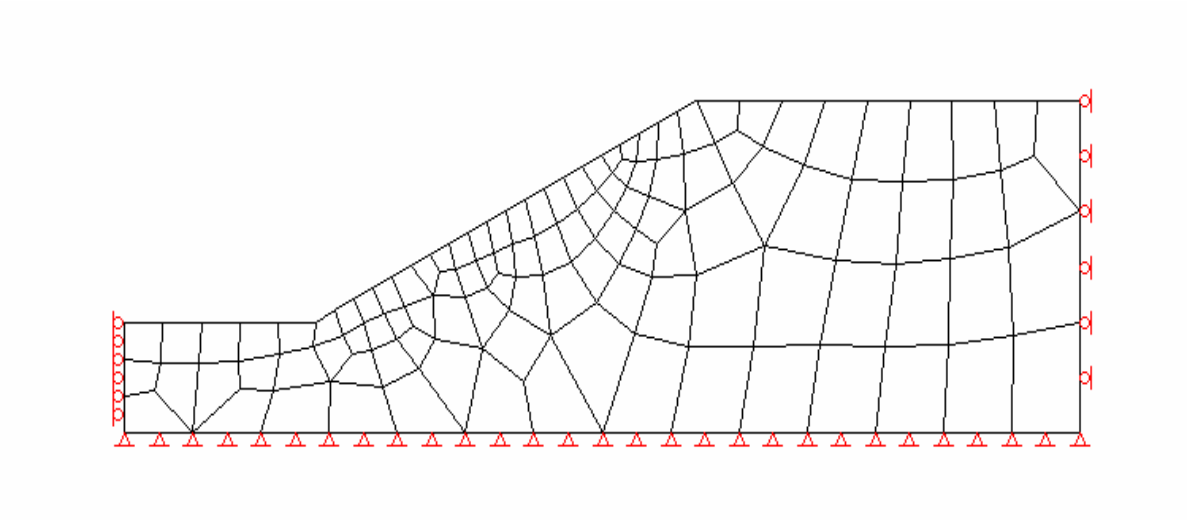

(b) Mesh with Q8 elements

Figure 3. Undeformed mesh

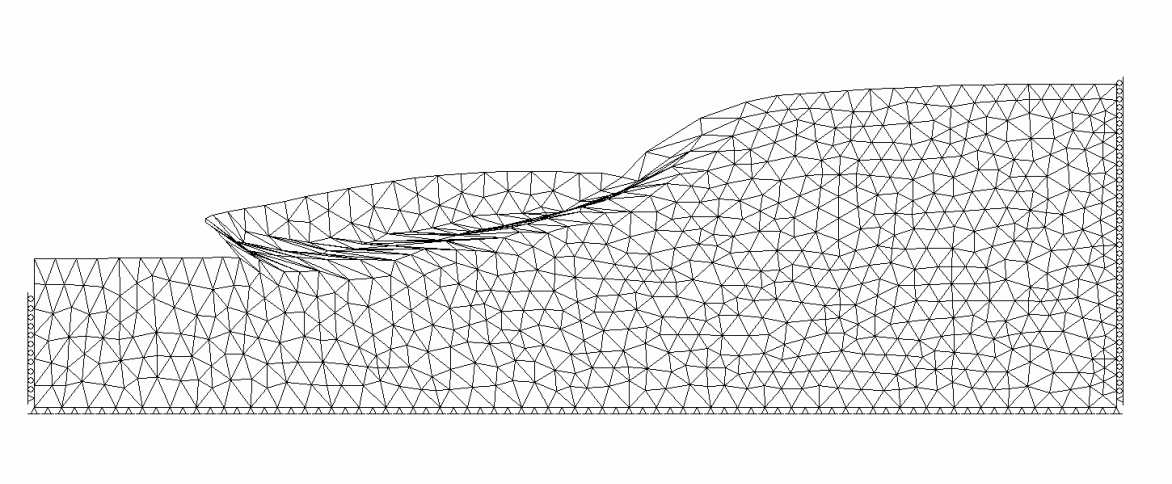

(a) Mesh with T6 elements

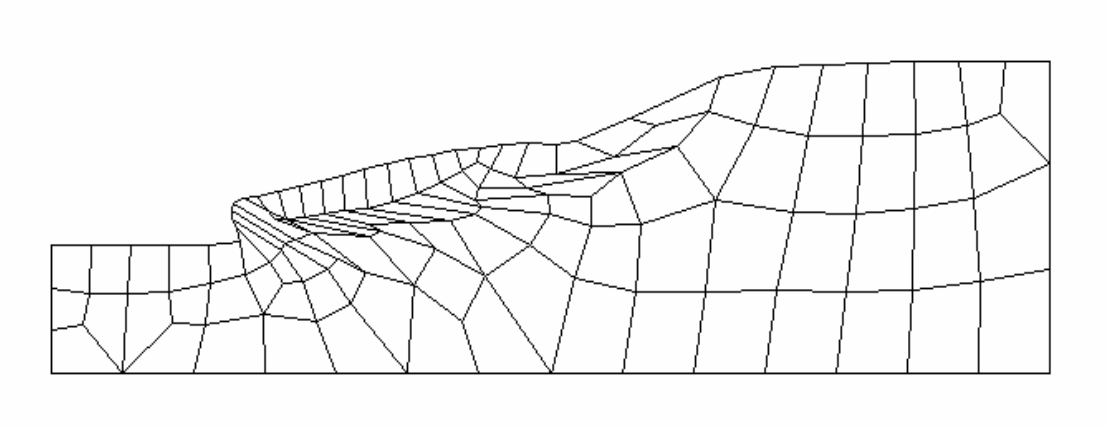

(b) Mesh with Q8 elements

Figure 4. Deformed mesh

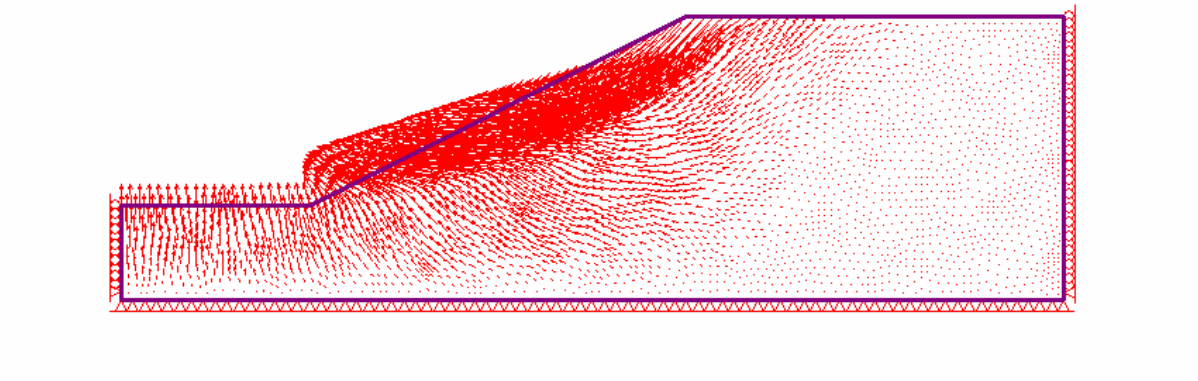

(a) Mesh with T6 elements

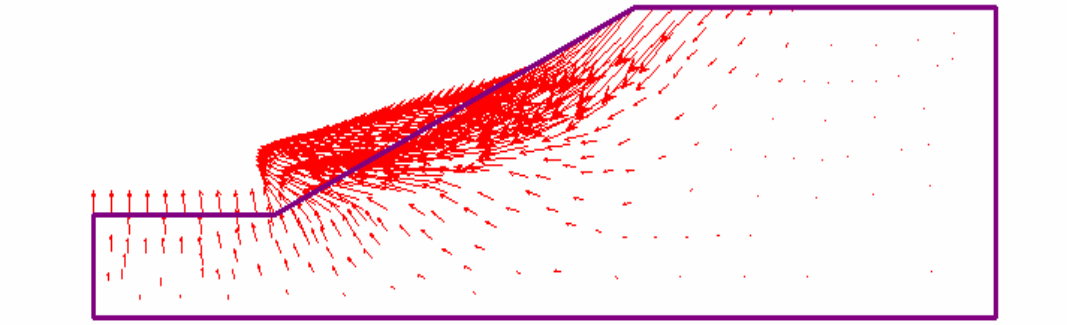

(a) Mesh with Q8 elements

Figure 5. Nodal displacement vectors

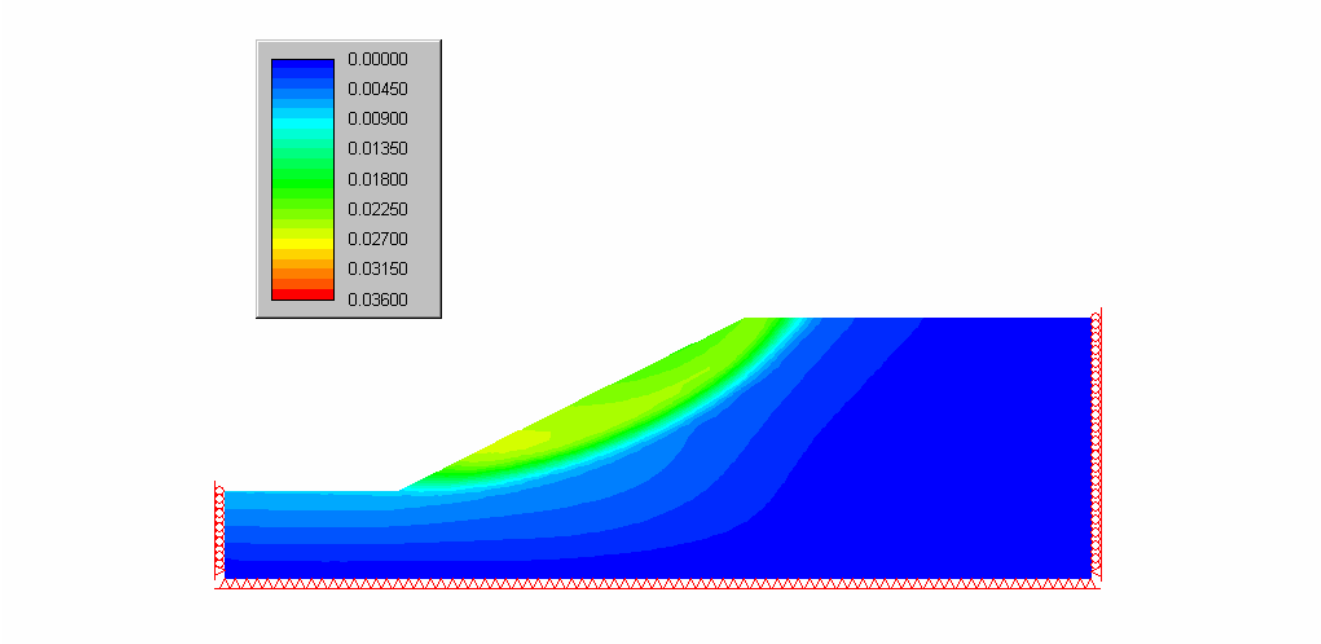

(a) Mesh with T6 elements

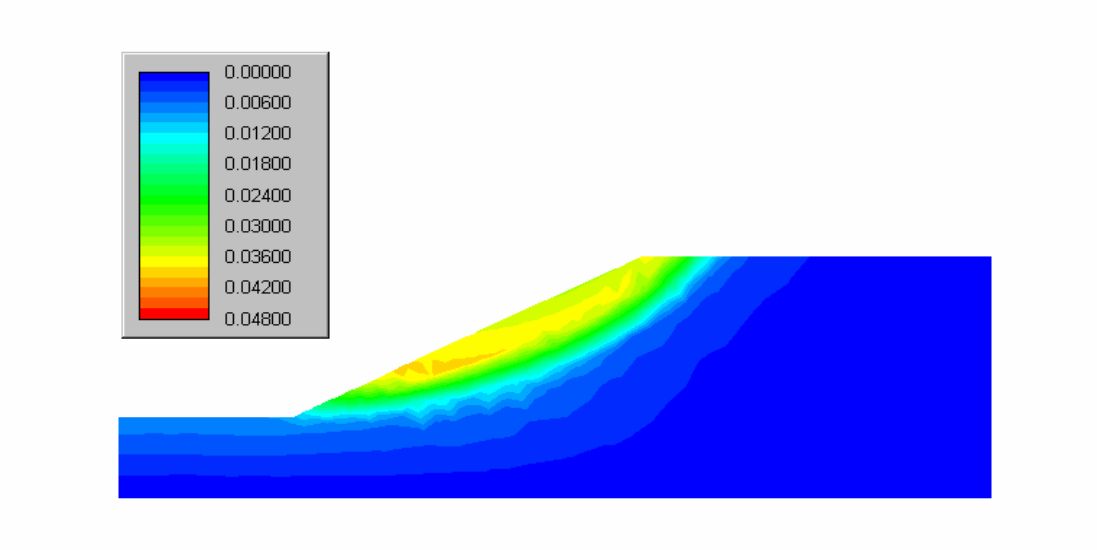

(b) Mesh with Q8 elements

Figure 6. Contours of total displacement

Table 4 shows the FOS results from *Phase*^{2} compared with several limit equilibrium methods

Table 4. FOS results for example 1

Janbu Corrected	Bishop	Spencer	GLE	*Phase*^{2} (T6)	*Phase*^{2} (Q8)
1.005	0.988	0.987	0.987	0.997	1.018

Undeformed meshes of the slope are presented in Figure 4. It is clear from Figure 5 and 6 that the slope is sliding along the "toe" of the slope.

Example 2. Non-homogeneous, three different soil layers slope.

This example comes from the *Slide* 3.0 verification manual (Problem #3). The slope has thee layers of non-homogeneous material. The geometry of the model is presented in Figure 7. The material properties of the three soils are shown in Table 5.

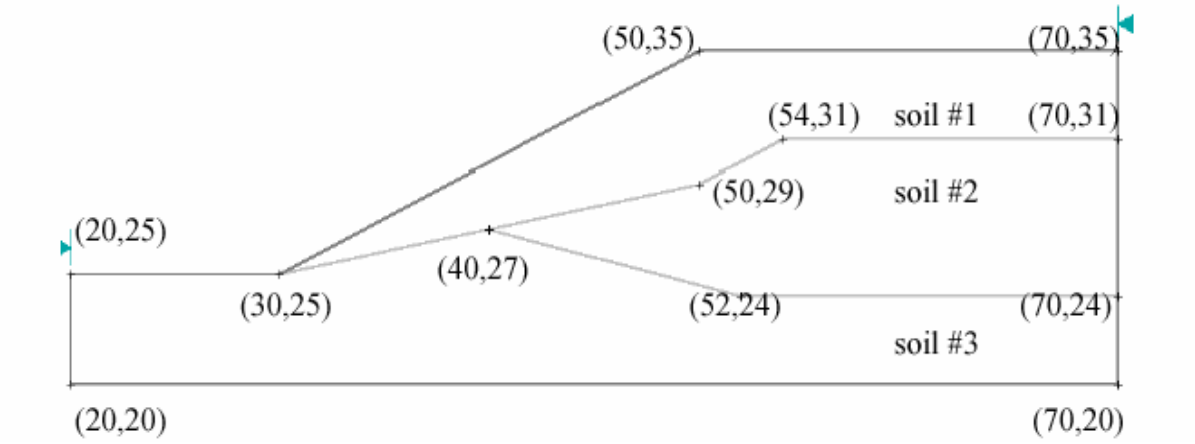

Figure 7. Geometry of the slope model

Table 5. Material Properties

	C (kN/m^2)	ϕ (degree)	γ (kN/m$^{3)}$
Soil #1	0.0	38.0	19.5
Soil #2	5.3	23.0	19.5
Soil #3	7.2	20	19.5

Figure 8 shows the two meshes used in the slope stability analysis. The total number of elements is 1442 for he first mesh that uses T6 elements. The second mesh discretized with 168 Q8 elements and is shown in Figure 8.

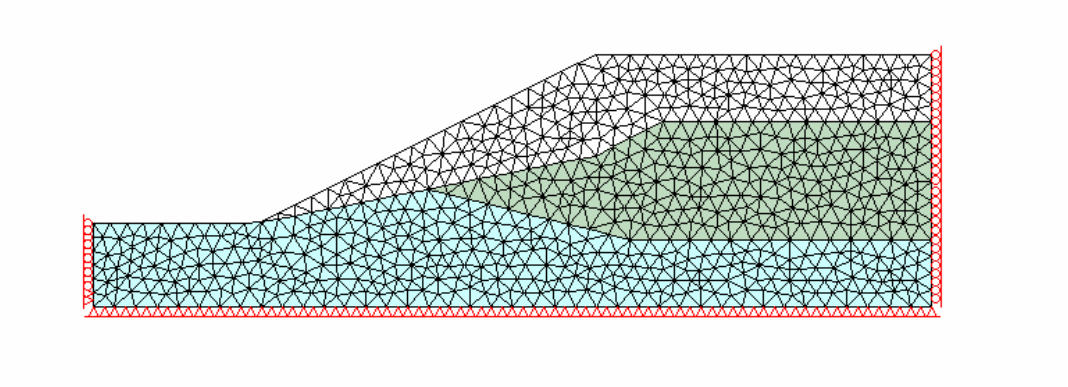

(a) Mesh with T6 elements

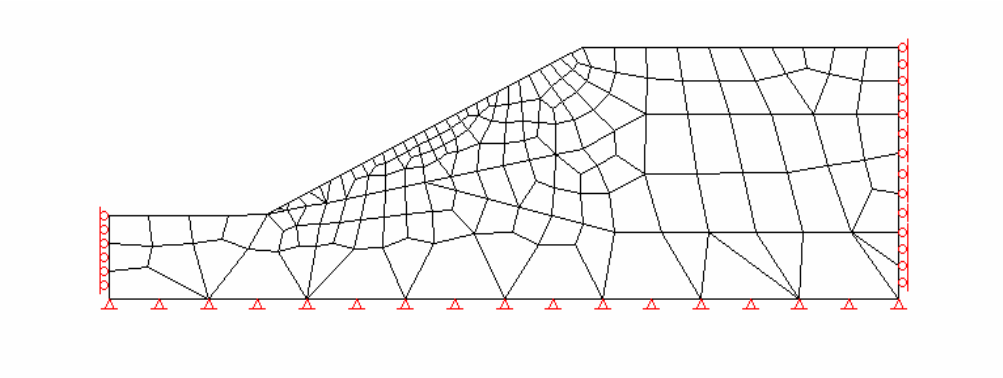

(b) Mesh with Q8 elements

Figure 8. Undeformed meshes for example 2

Table 6 shows the FOS results from *Phase*^{2} compared with several limit equilibrium methods

Table 6. FOS results for example 2

Janbu Corrected	Bishop	Spencer	GLE	*Phase*^{2} (T6)	*Phase*^{2} (Q8)
1.393	1.410	1.380	1.398	1.385	1.389

It is shown in Table 6 that the difference in *FOS* for T6 and Q8 analysis is less that 0.4%. Phase2 results compared well with different limit equilibrium methods. The deformed meshes, nodal displacement vectors and the contours of sliding surface are presented in Figures 9, 10 and 11 respectively.

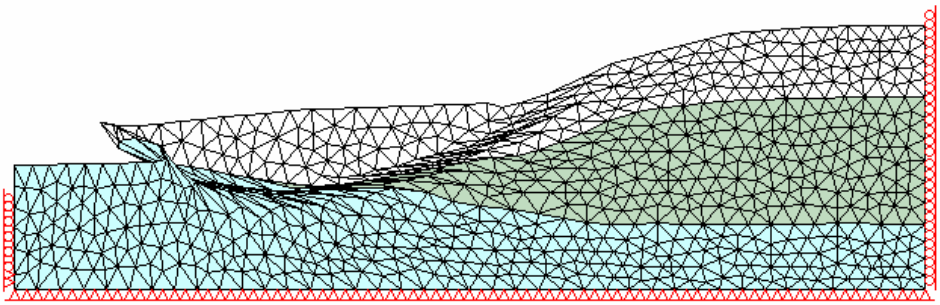

(a) Mesh with T6 elements

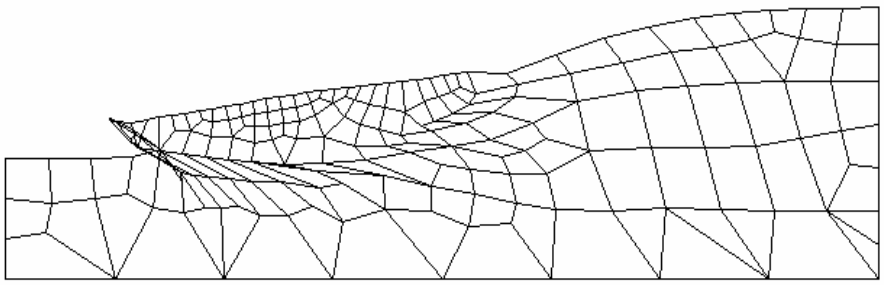

(b) Mesh with Q8 elements

Figure 9. Deformed meshes for example 2

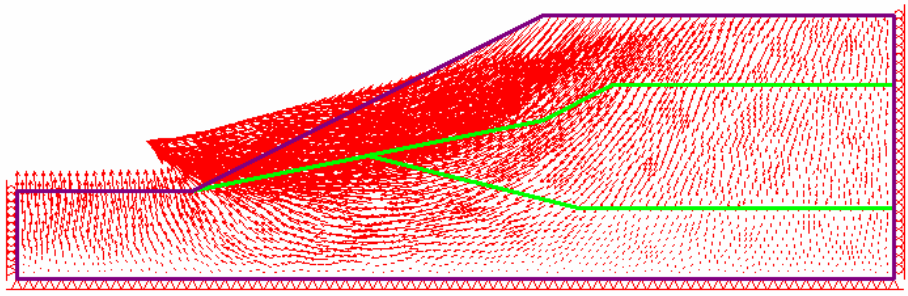

(a) Mesh with T6 elements

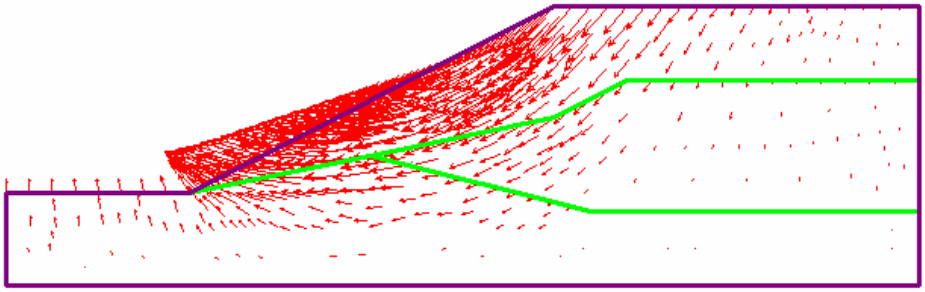

(a) Mesh with Q8 elements

Figure 10. Displacements vectors for example 2

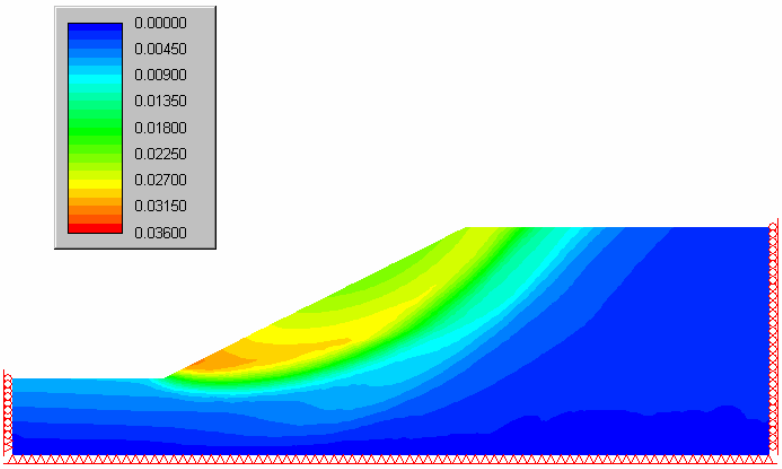

(a) Mesh with T6 elements

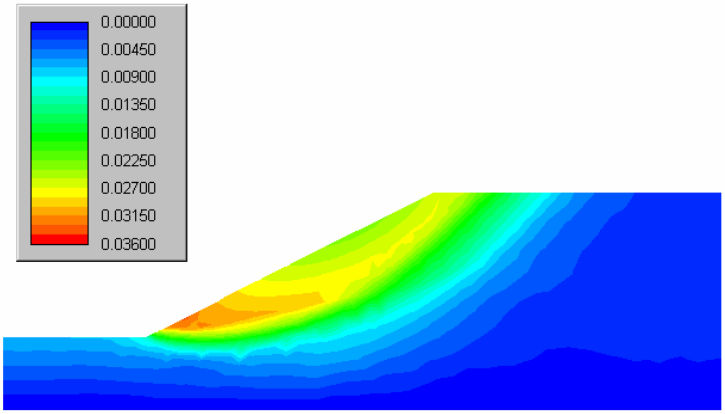

(b) Mesh with Q8 elements

Figure 11. Contours of total displacements

Example 3. An undrained clay slope failure with a thin weak layer

This example demonstrates a stability analysis of a slope of undrained clay. This example is taken from Griffiths' paper (Griffiths, 1999). The slope model consists of a thin layer of week material. The weak layer runs parallel to the slope and then turns to be horizontal in the toe zone. The presence of this thin weak layer in the slope influences the stability of slope. In this example, different values of C_{u2}/C_{u1} was considered.

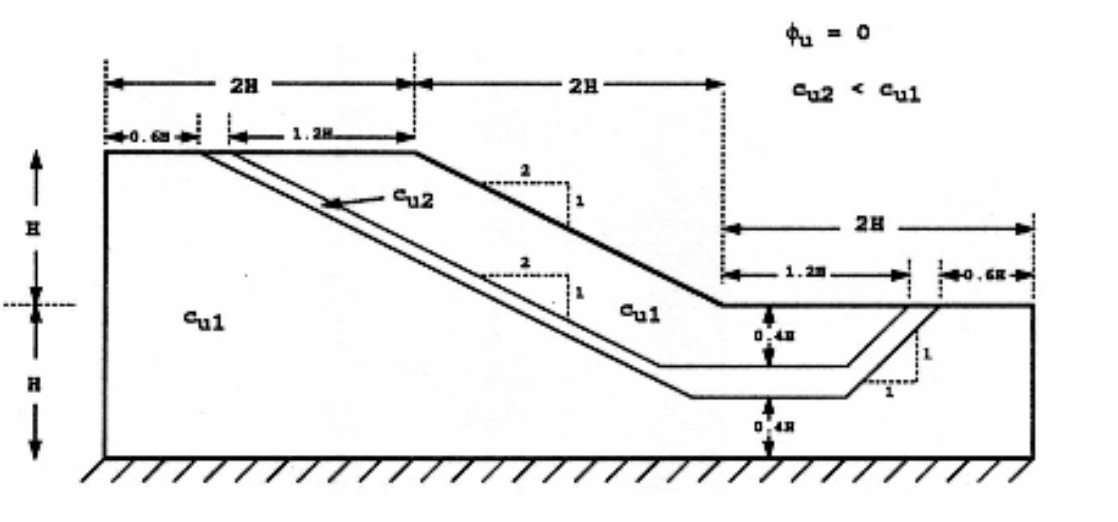

Figure 12. Undrained clay slope with a foundation layer including a thin weak

The geometry of the slope model is presented in Figure 12. The slope height is 10 meters and $C_{u1}/\gamma H$ ratio is taken as 0.25. Table 7 presents the material properties for the slope model.

Table 7. Slope material properties

C_{u1} (kN/m^2)	ϕ (degree)	γ (kN/m$^{3)}$	C_{u2} (C_{u2}/C_{u1}=0.6)	C_{u2} (C_{u2}/C_{u1}=1)	C_{u2} (C_{u2}/C_{u1}=0.2)
0.05	0.0	20.0	0.05	0.03	0.01

In this example, first mesh discretized with T6 2644 elements and the second mesh discretized with 377 Q8 elements. Figure 13 shows the two meshes.

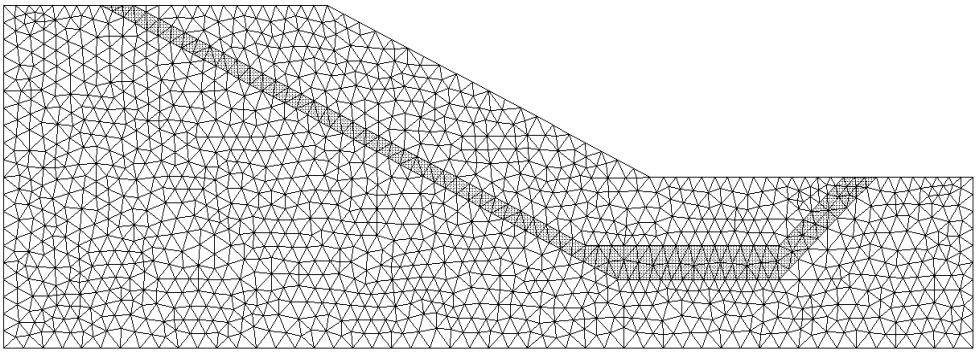

(a Mesh with T6 elements

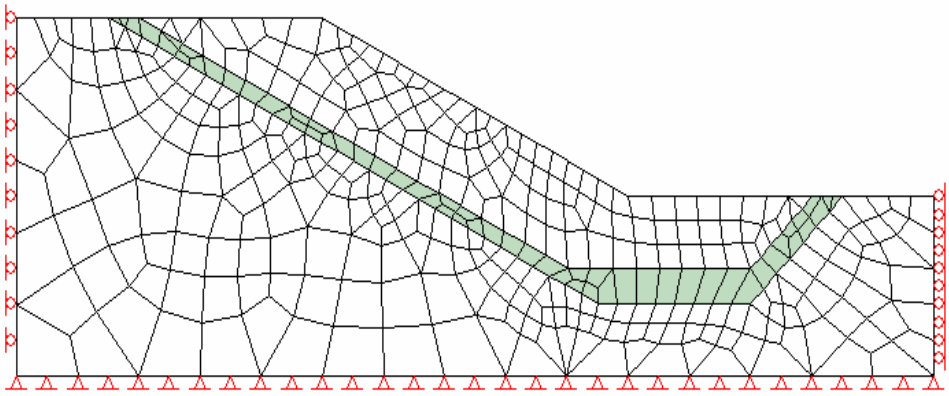

(b) Mesh with Q8 elements

Figure 13. Undeformed meshes

Case 1: $C_{u2}/C_{u1}=1$

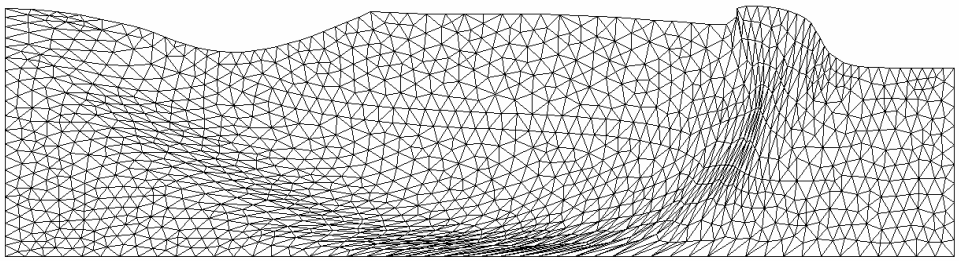

(a) Mesh with T6 elements (*FOS*=1.45)

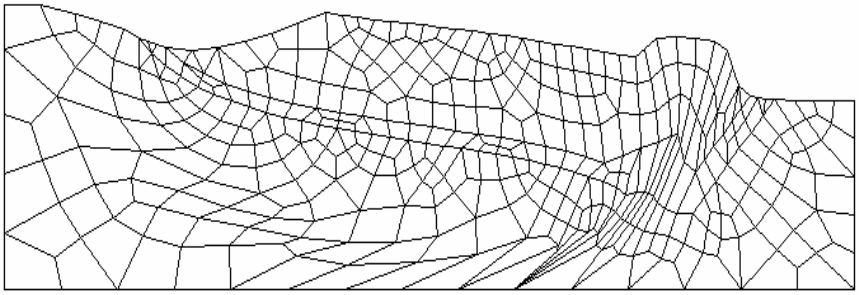

(b) Mesh with Q8 elements (*FOS*=1.47)

Figure 14. Deformed meshes

Case 1: $C_{u2}/C_{u1}=1$

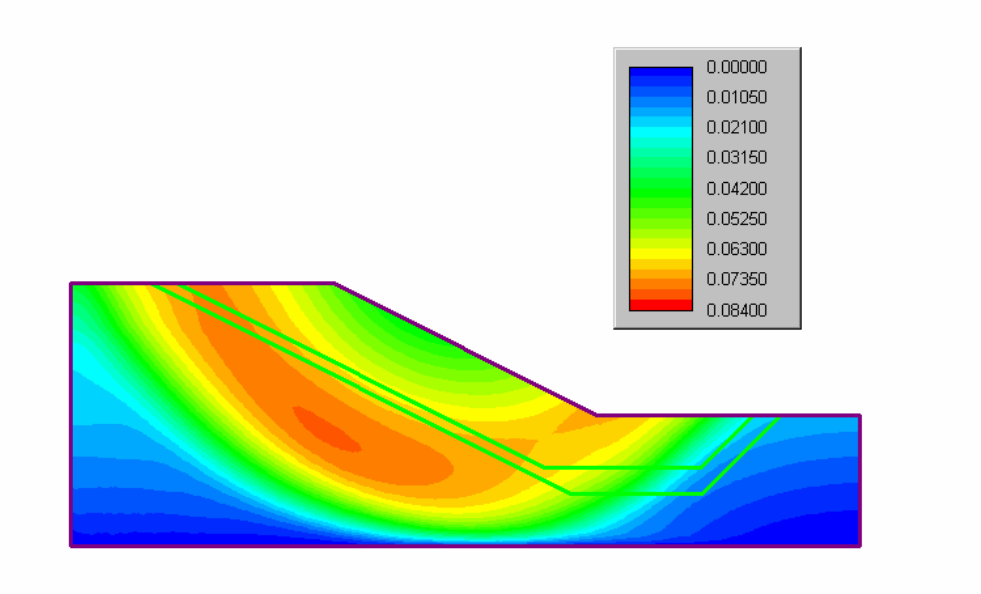

(b) Mesh with T6 elements

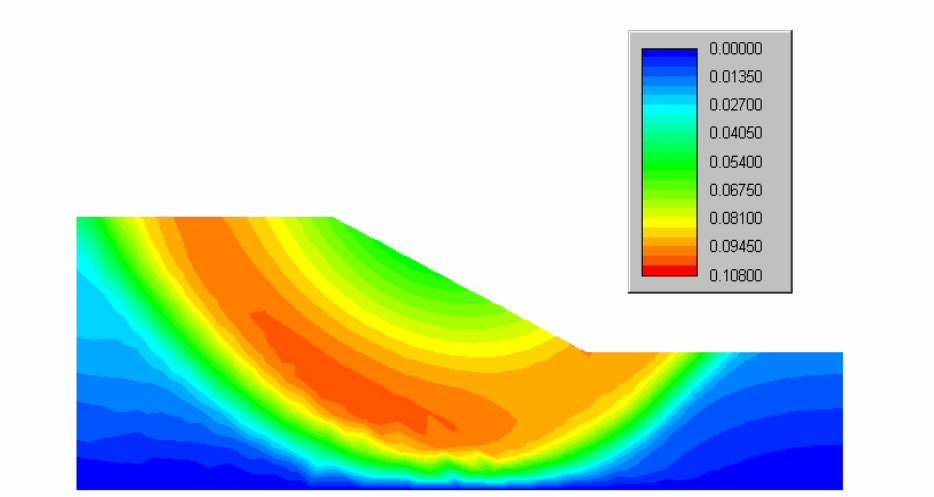

(b) Mesh with Q8 elements

Figure 15. Contours of total displacements

Case 1: C_{u2}/C_{u1}=0.6

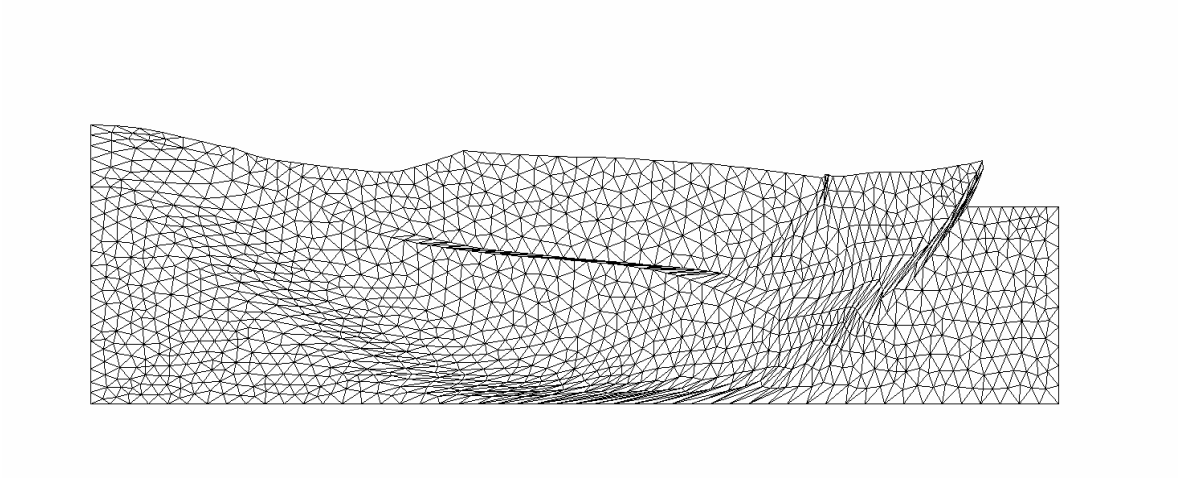

(a) Mesh with T6 elements (*FOS*=1.35)

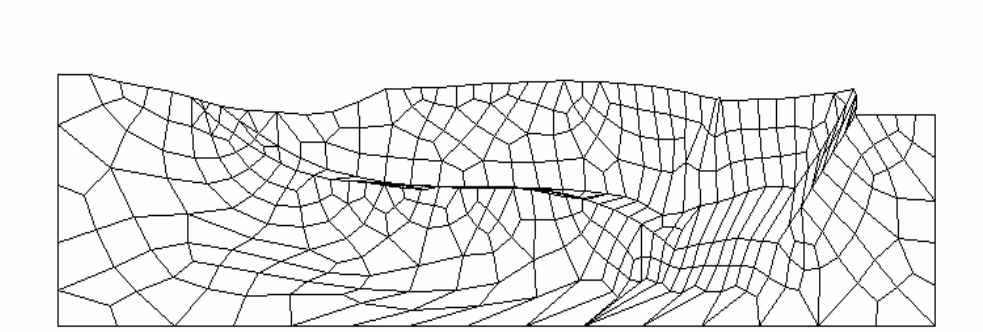

(b) Mesh with Q8 elements (*FOS*=1.35)

Figure 16. Deformed meshes

Case 1: C_{u2}/C_{u1}=0.6

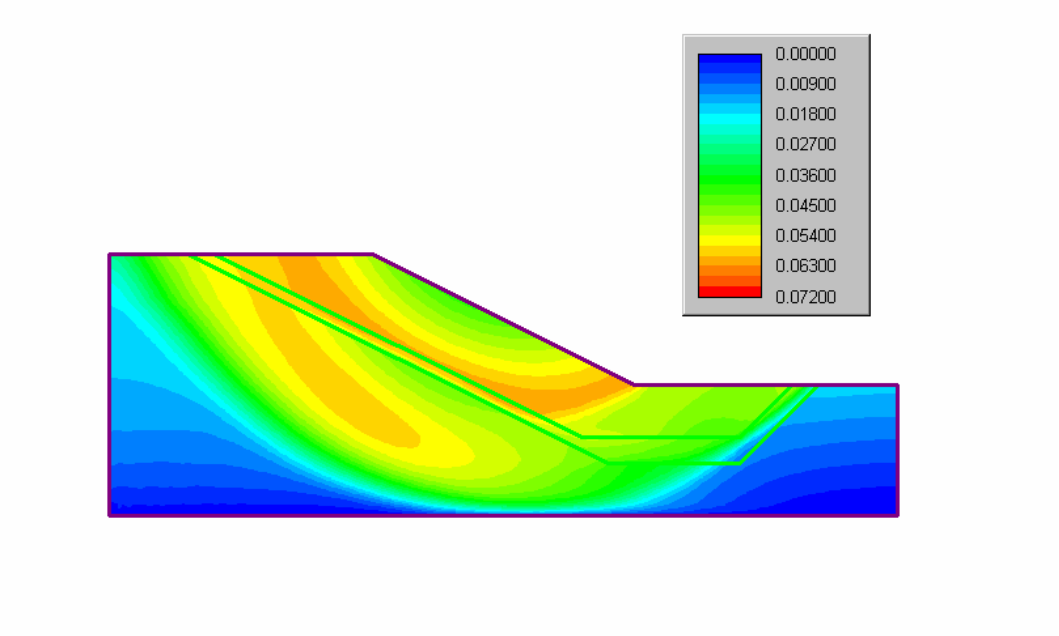

(b) Mesh with T6 elements

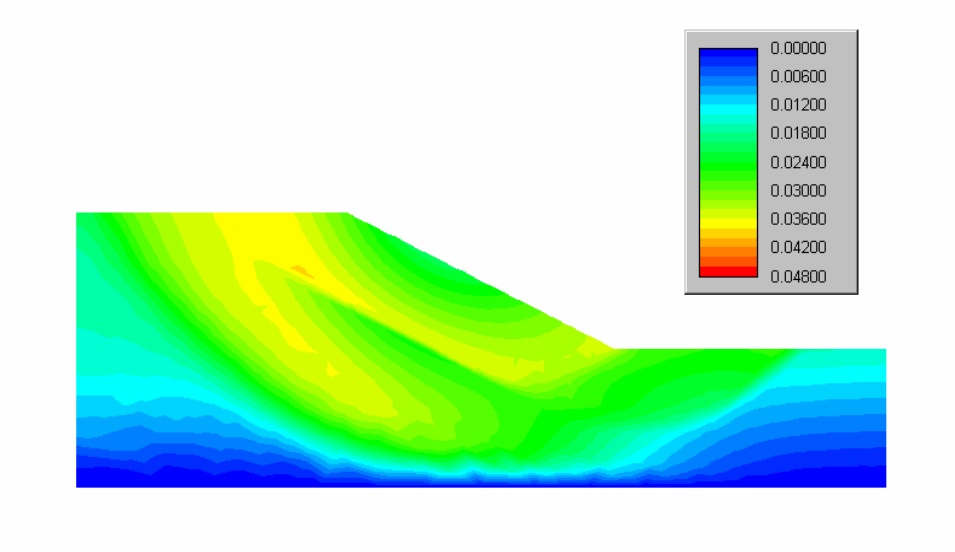

(b) Mesh with Q8 elements

Figure 17. Contours of total displacements

Case 1: C_{u2}/C_{u1}=0.2

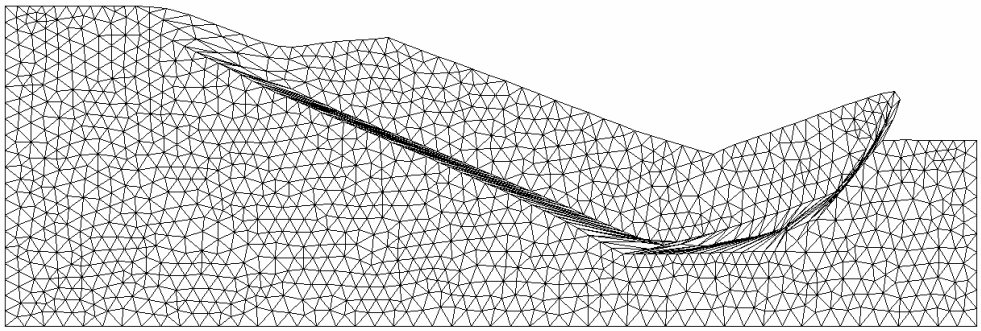

(a) Mesh with T6 elements (*FOS*=0.62)

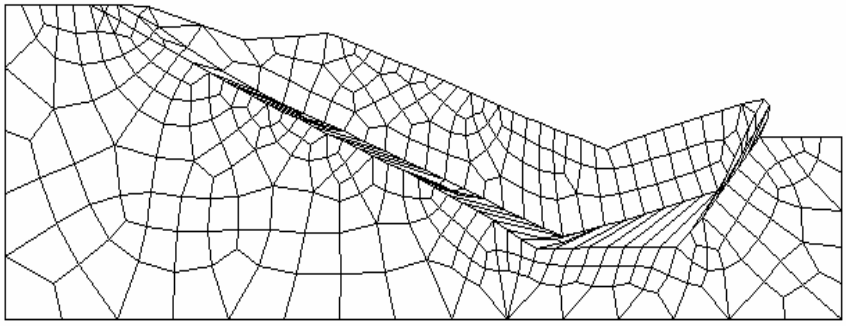

(b) Mesh with Q8 elements (*FOS*=0.59)

Figure 18. Deformed meshes

Case 1: C_{u2}/C_{u1}=0.2

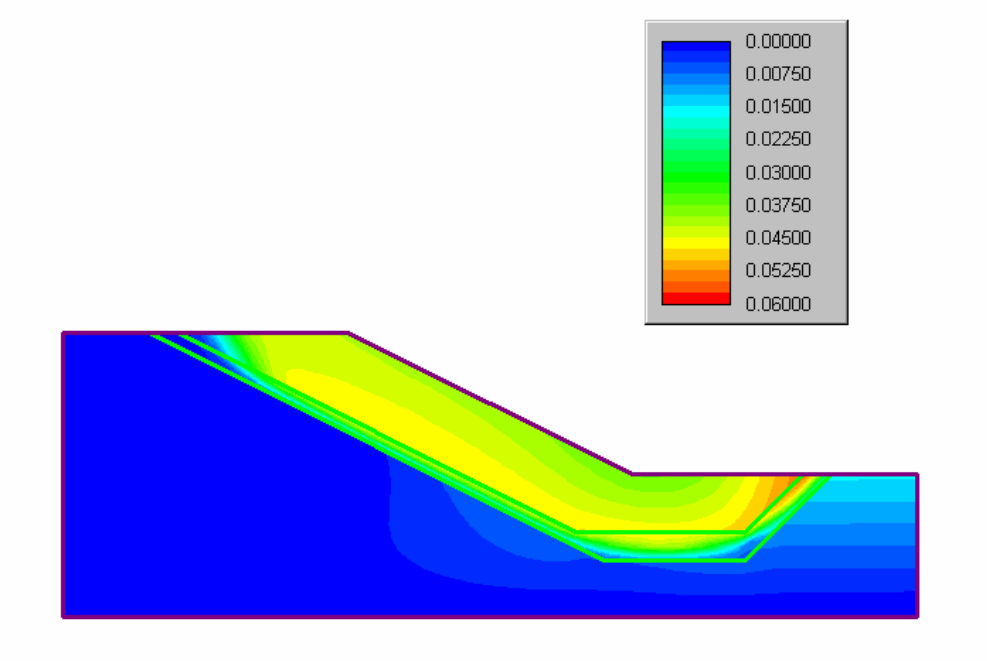

(a) Mesh with T6 elements

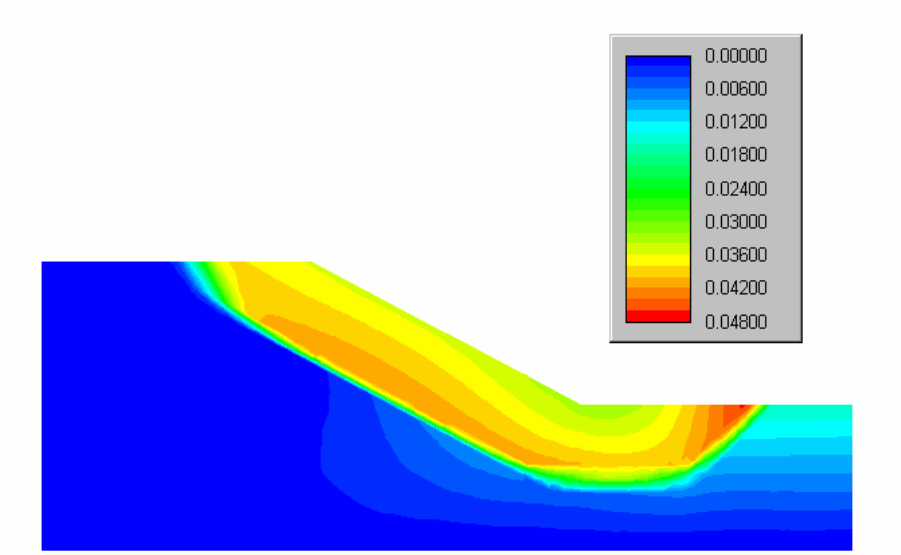

(b) Mesh with Q8 elements

Figure 19. Contours of total displacements

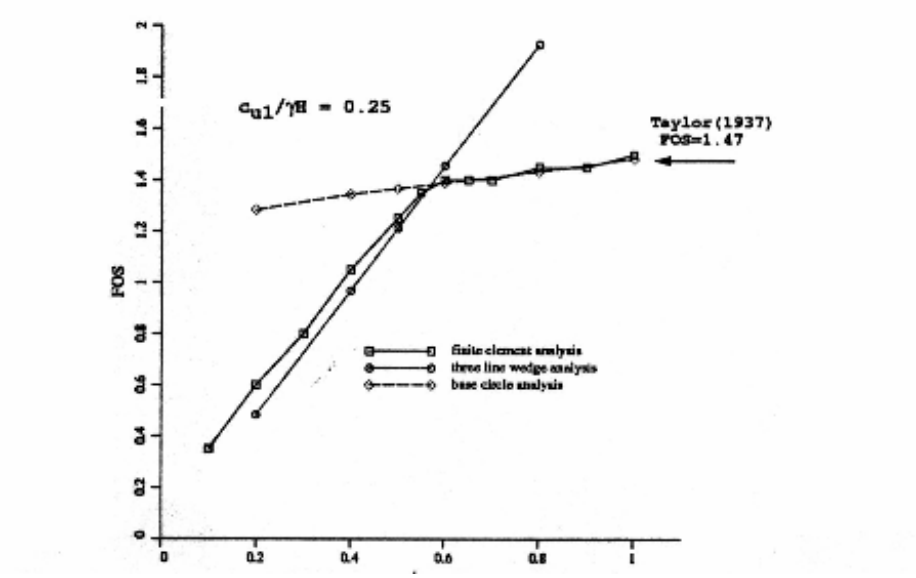

Figure 20. *FOS* for different values of C_{u2}/C_{u1} (Griffiths, 1999)

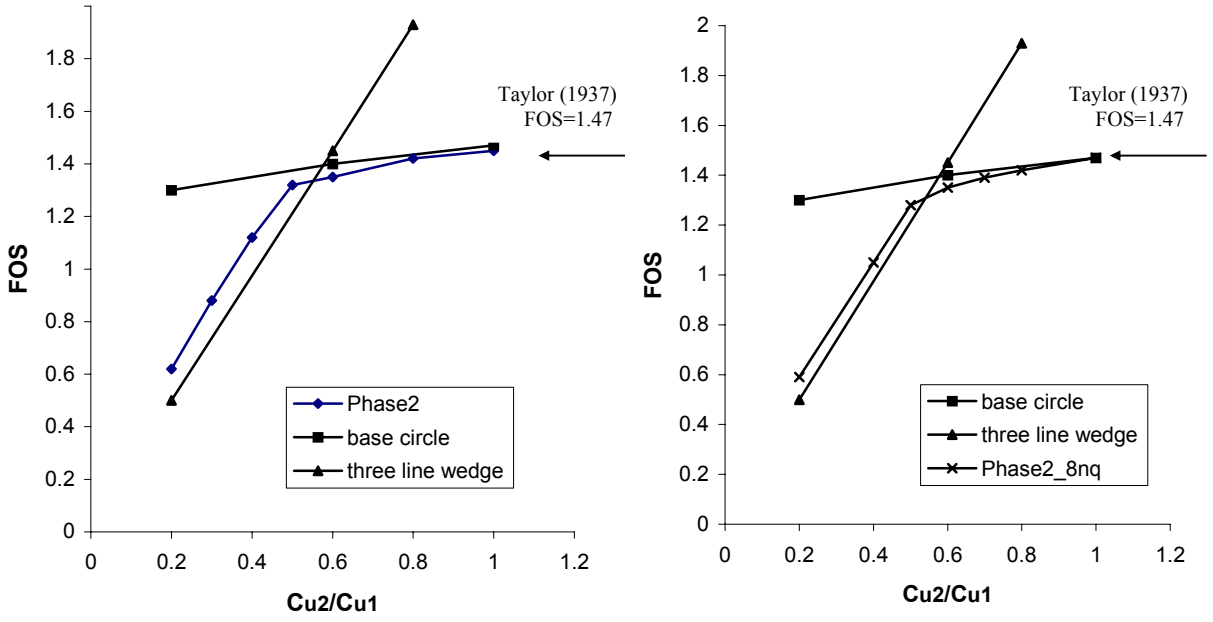

(a) T6 elements (b) Q8 elements

Figure 21. *FOS* for different values of C_{u2}/C_{u1} from *Phase*^{2}

Seven cases are studied in this example using T6 and Q8 elements. Three cases used different cohesion strength ratio for the thin layer compared to the slope material. These ratios were 0.2, 0.6 and 1.0. Figures 14-19 show the deformed meshes and the total displacements contours for the two meshes.

Figures 20-21 shows three results obtained using finite element analysis and Janbu's method assuming both circular (base failure) and three line wedge mechanism following the path of weak layer. *Phase*^{2} results are compared well with Griffiths' FE results as it is shown in Figures 20-21. For the homogeneous slope model (C_{u1}/C_{u2}=1.0), *FOS* was close to the Taylor solution (Taylor, 1937). The failure mechanism showed a circular slip which confirms the expectation.

For the case of $C_{u2}/C_{u1}\approx 0.6$, a distinct change is observed. It shows that for $C_{u2}/C_{u1}>0.6$, the base failure mechanism governs the slope behaviors and the weaker thin layer doesn't influence the factor of safety. For $C_{u2}/C_{u1}<0.6$, the thin weak layer mechanism controls the slope behavior and the *FOS* falls linearly. The obvious difference between *Phase*^{2} and Griffiths' results is that the point of distinct change moves to the position of $C_{u2}/C_{u1}\approx 0.5$. Figure 21 shows that both T6 and Q8 are very similar.

The failure mechanisms of T6 and Q8 for C_{u2}/C_{u1}=0.2, C_{u2}/C_{u1}=0.6 and C_{u2}/C_{u1}=1.0 are shown in Figure 14-19. For the case of C_{u2}/C_{u1}=0.2, figures 18-19 indicate a highly concentrated non-circular mechanism moving along the path of the thin weak layer. The strength of the thin layer is 60% of the surrounding soil. The sliding surface of the slope failure happens in the thin weak layer and the circular failure (base failure). There failure mechanisms are same as those obtained by Griffiths.

Example 4. Undrained clay slope with a foundation layer

The slope geometry is taken similar to the slope geometry of example 3. The slope model consists of two soil material, the shear strength of the foundation layer is different from that of the slope. The geometry of the slope model is presented in Figure 22. The material properties are presented in Table 8.

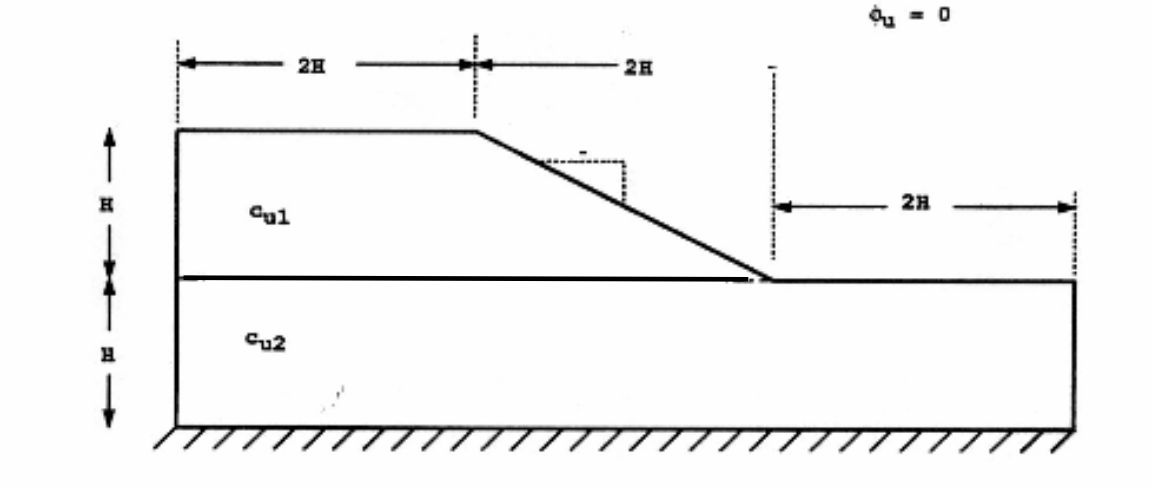

Figure 22. Model geometry of Example 4

Table 8. Slope material properties

C_{u1} (kN/m^2)	ϕ (degree)	γ (kN/m$^{3)}$	C_{u2} (C_{u2}/C_{u1}=0.5)	C_{u2} (C_{u2}/C_{u1}=1)	C_{u2} (C_{u2}/C_{u1}=1.5)	C_{u2} (C_{u2}/C_{u1}=2)
0.05	0.0	20.0	0.025	0.05	0.075	0.1

Two meshes are used. The first mesh consists of 2538 T6 elements and the second uses 241 Q8 elements. Undeformed meshes of the two models are presented in Figure 23.

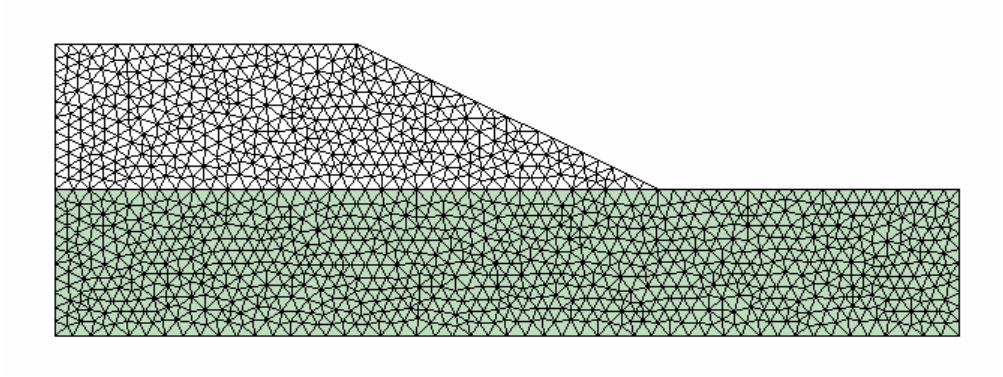

(a) Mesh with T6 elements

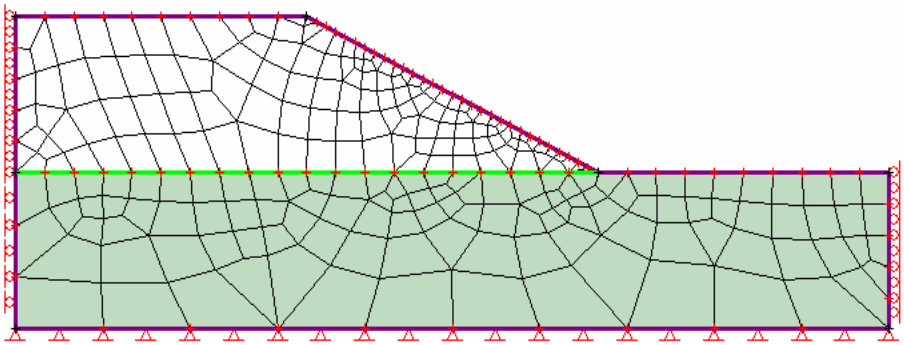

(b) Mesh with Q8 elements

Figure 23. Undeformed meshes

Figure 24-25 show the deformed mesh for different C_{u1}/C_{u2} ratios for the mesh of T6 and Q8 elements respectively.

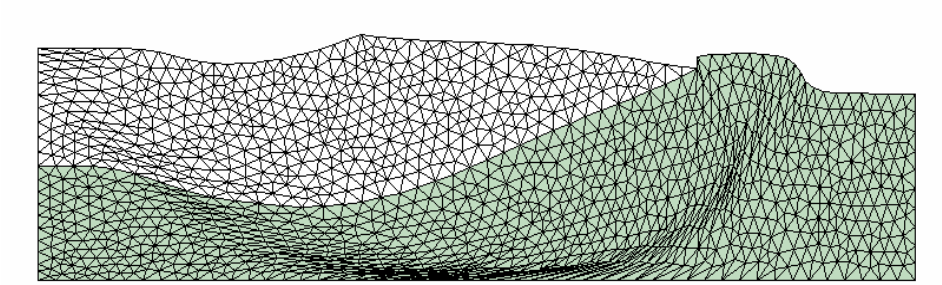

(a) C_{u2}/C_{u1}= 0.5, *FOS*=0.82

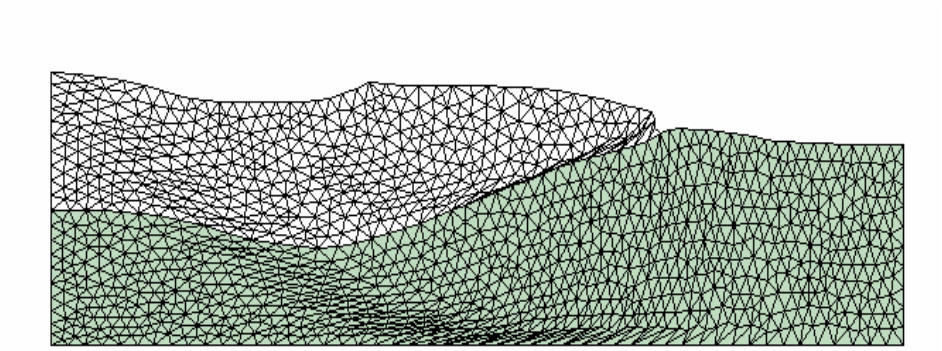

(b) C_{u2}/C_{u1}= 1.5, *FOS*=2.03

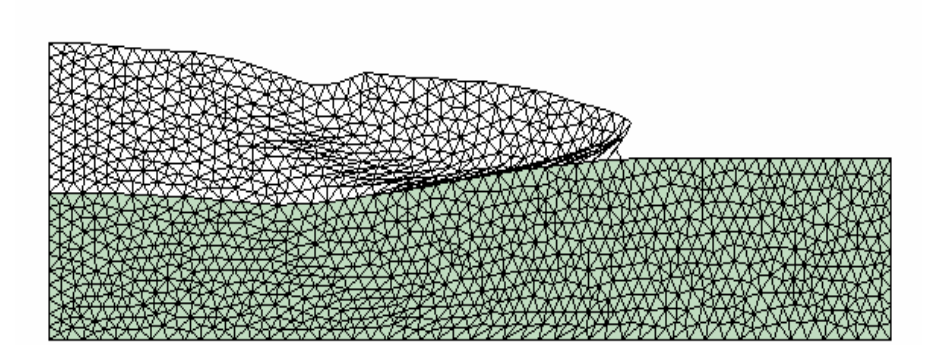

(c) C_{u2}/C_{u1}= 2.0, *FOS*=2.24

Figure 24. Deformed mesh for T6 elements

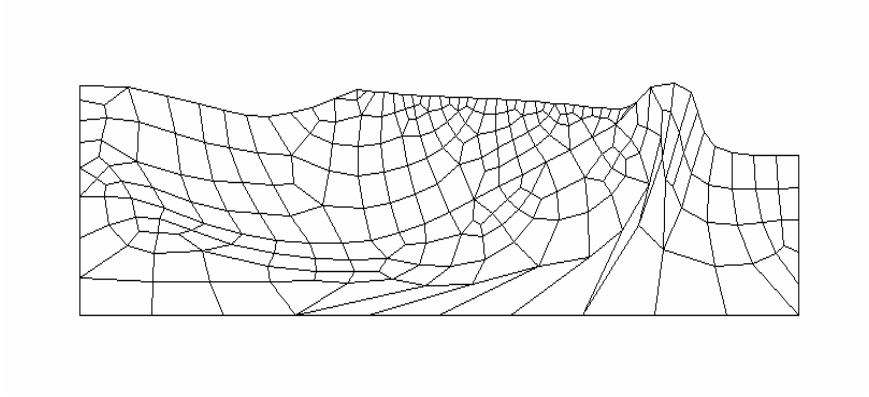

(a) C_{u2}/C_{u1}= 0.5, *FOS*=0.84

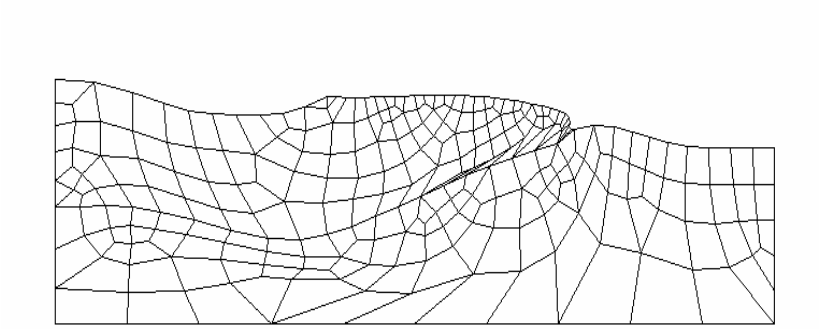

(b) C_{u2}/C_{u1}= 1.5, *FOS*=2.03

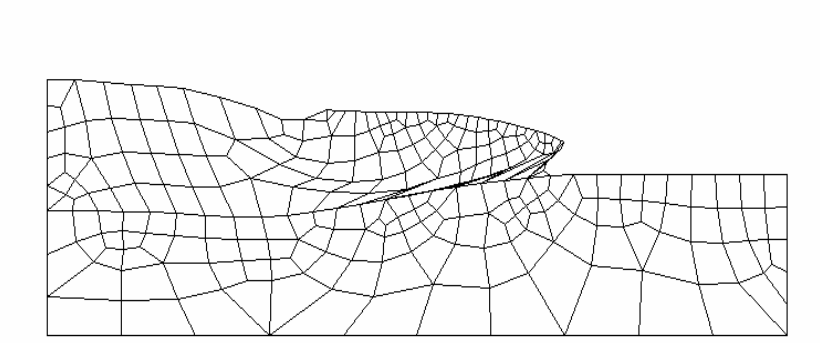

(c) C_{u2}/C_{u1}= 2.0, *FOS*=2.10

Figure 25. Deformed mesh for Q8 elements

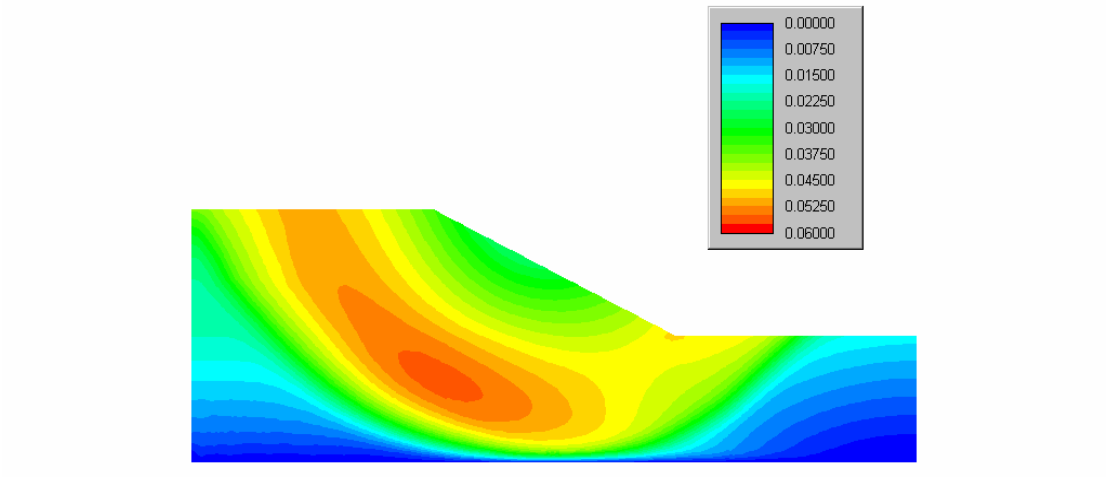

(a) C_{u2}/C_{u1}= 0.5

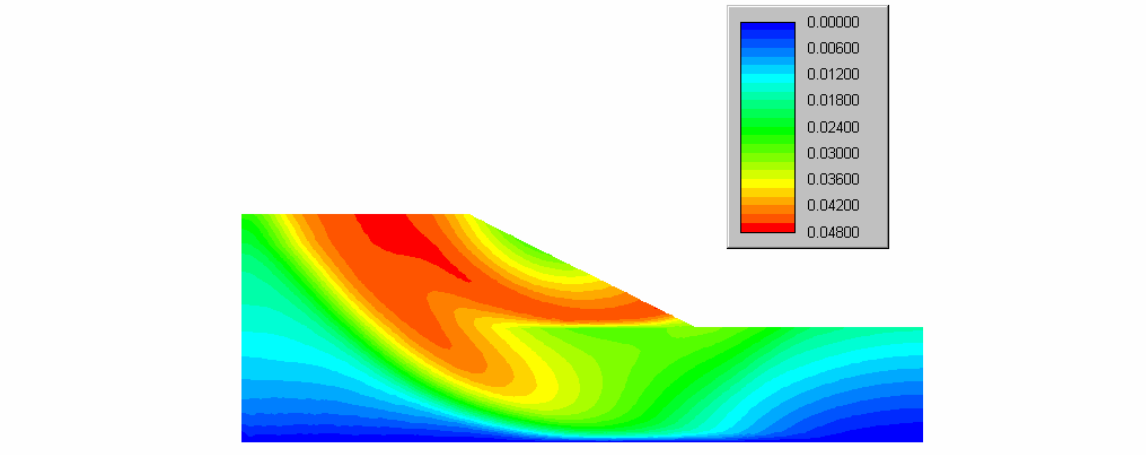

(b) C_{u2}/C_{u1}= 1.5

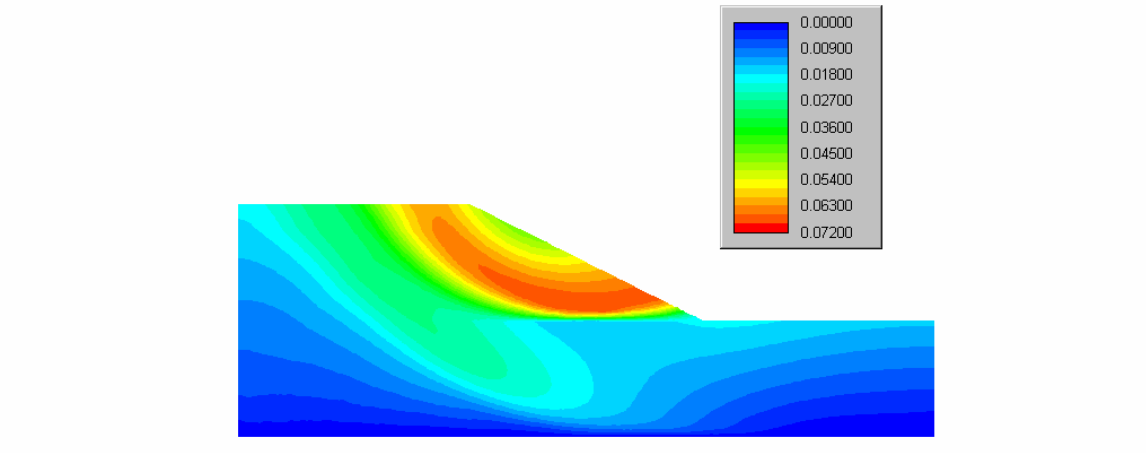

(c) Cu2/Cu1 = 2.0

Figure 26. Contours of total displacement (T6 elements)

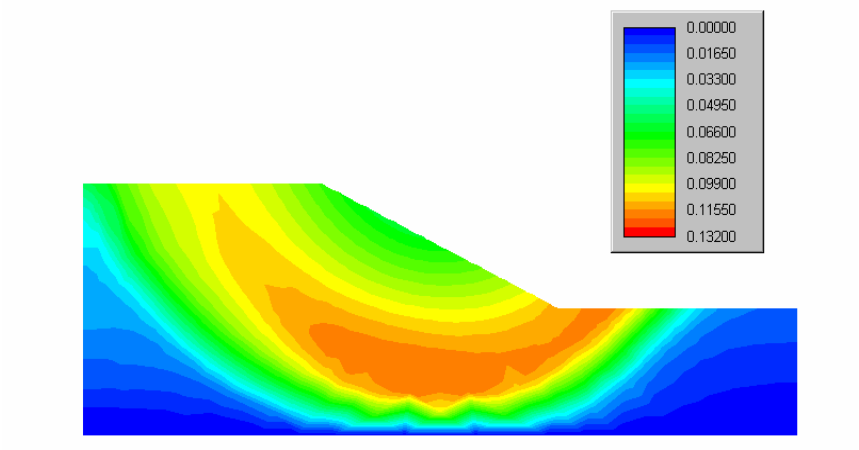

(a) C_{u2}/C_{u1}= 0.5

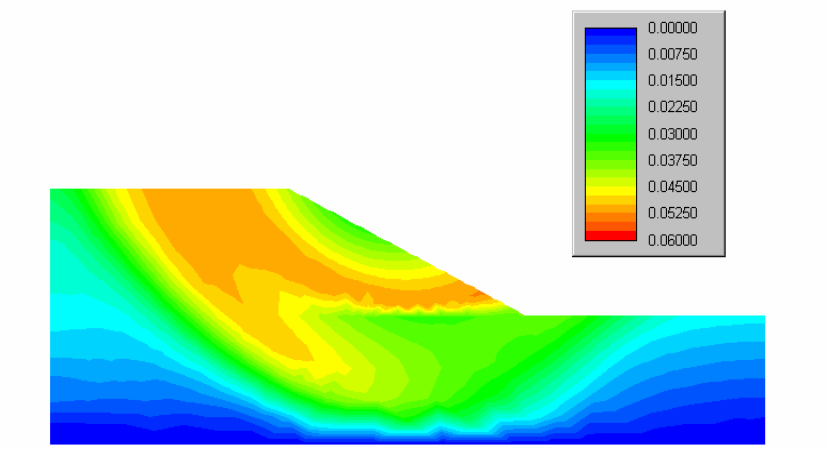

(b) C_{u2}/C_{u1}= 1.5

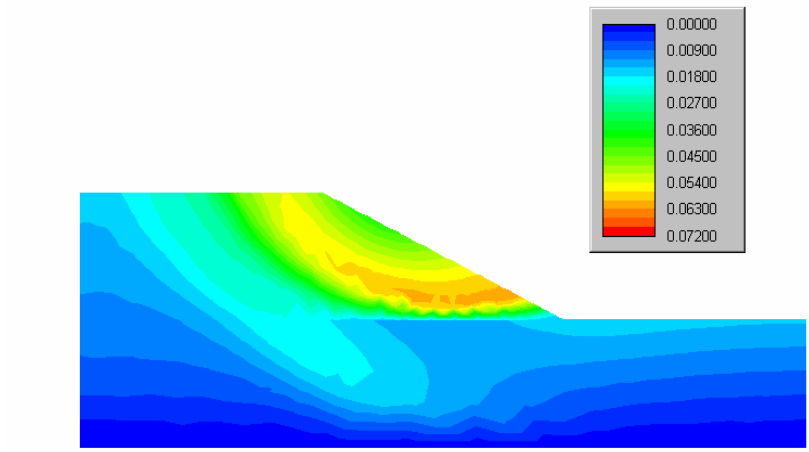

(c) Cu2/Cu1 = 2.0

Figure 27. Contours of total displacement (Q8 elements)

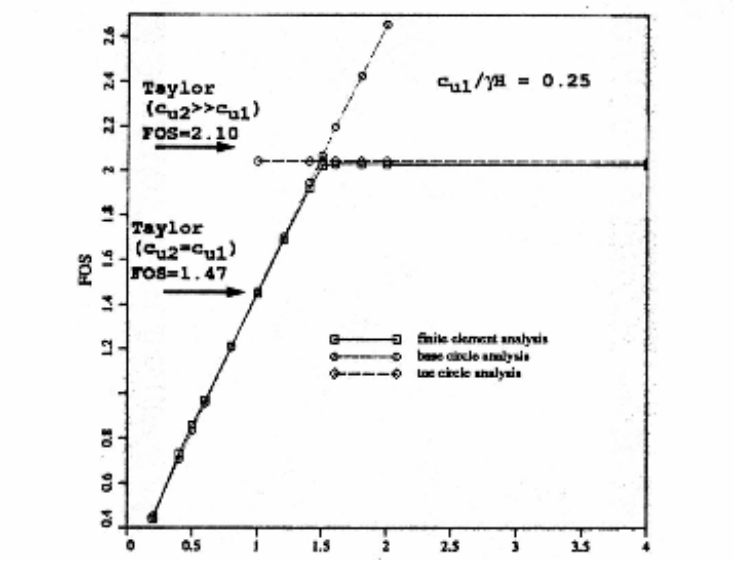

Figure 28. *FOS* for different values of C_{u2}/C_{u1} (Griffiths, 1999)

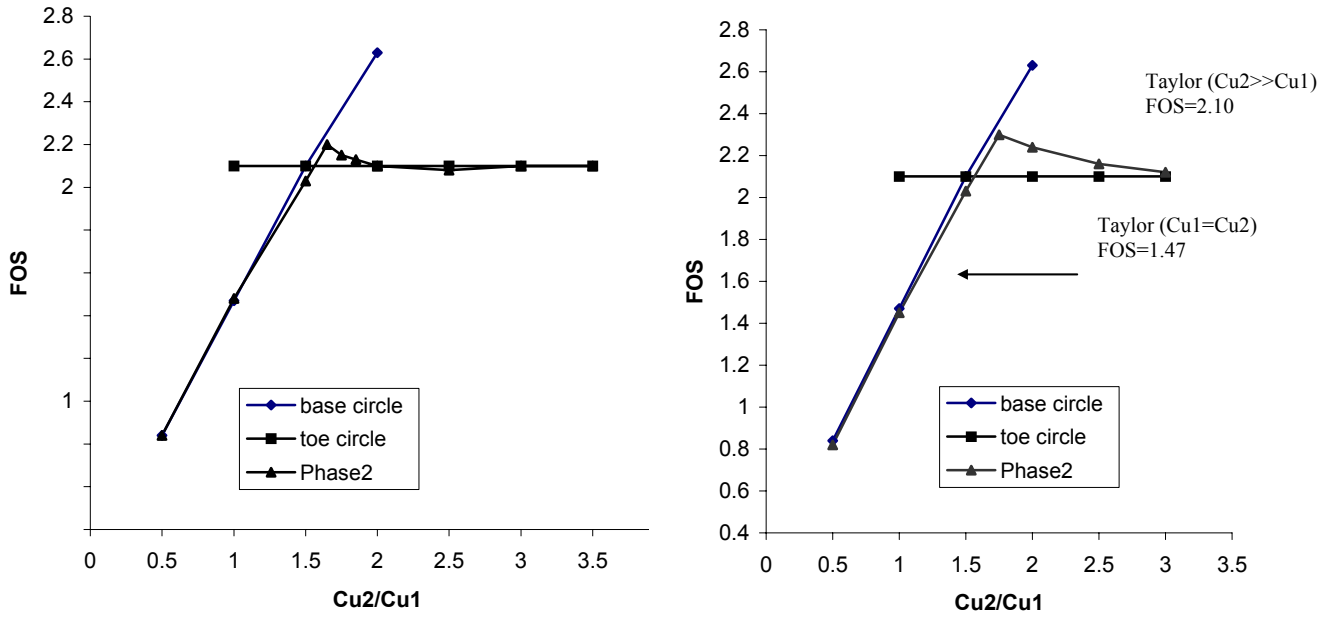

(a) T6 elements (b) Q8 elements

Figure 29. *FOS* for different values of C_{u2}/C_{u1} from *Phase*^{2}

Figures 24-27 show the deformed mesh and the total displacement contours for different slope cases. It is clear from these figures that the values of C_{u2}/C_{u1} will dominate the failure mechanism. A deep-seated base failure mechanism is dominated when $C_{u2}<<C_{u1}$ while a shollow 'toe' faile mechanis is noticed for the case when $C_{u2}>>C_{u1}$. The deformed meshes compared well with the results presented by Griffiths.

Figure 29 shows the variation of *FOS* verses different values of C_{u2}/C_{u1} for the two meshes. It is also plotted in Figure 29 the values of Taylor's solution. Figure 29 shows that there is a distinct translation point occuring at C_{u2}/C_{u1} = 1.5. This value represnts the seperation between two failure mechanism. This confirms the behaviour presented in Figures 24-27. Generally, *Phase*^{2} results compared very well with those presented in Griffiths work.

5. Conclusions

Slope stability represents an area of geotechnical analysis in which finite element method offrers real benefits over limit equilibrium methods. The ease of use of *Phase*^{2} software helped in exploring the benefit of using finite element technique for slope stability problems. *Phase*^{2} results compared very well with previous finite element work presented by Griffiths. Limit equilibrium methods calculated using *Slide* software are also helped in verifying *Phase*^{2} results. Although this work used only Mohr-Coulomb failure criterion for the model material, extension the work to cover more material models are also possible since different material models are already incorporated in *Phase*^{2}. Only reducing strength procedure is used in the present work and more methods will be looked at in the near future.

The present study was carried out before introducing *Phase*^{2} version 5.0 and therefore all examples are presented without including ground water effect. Incorporating pore water pressure enables *Phase*^{2} to cover a wider range of practical slope stability problems.

Reference:

J. M. Duncan, State of the art: limit equilibrium and finite-element analysis of slopes. J. Geotech. Engng, ASCE 122, **7**, 577-597 (1996).

D. V. Griffiths, Stability analysis of highly variable soils by elasto-plastic finite Elements (1999)

Rocscience Inc., Phase^2 user's guide Version 2.1 (2002)

I. M. Smith and D.V.Griffiths, Programming the Finite Element Method. Third Edition 1998 John Wiley & Sons

Rocscience Inc., Slide User's Guide (2003)

C.C. Swan, Y.K. Seo, Limit State Analysis of Earthen Slopes Using Dual Continuum/FEM Approaches. Int. J. Numer. Anal. Meth. Geomech., **23**, 1359-1371 (1999)

D. W. Taylor, Stability of earth slopes. J. Boston Soc. Civ. Eng, **24**, 197-246 (1937).

Appendix A

Additional Examples

In this Appendix, several examples are presented that compare *Phase*^{2} Finite Element results with limit equilibrium results from *Slide*. You can download the example files from: http://www.rocscience.com/downloads/phase2/SlopeStabilityExamples.zip

I. Example 1 (Slide verification example #15)

This model is taken from Arai and Tagyo (1985) example#2 and consists of a layered slope where a layer of low resistance is interposed between two layers of higher strength. A number of other authors have also analyzed this problem, notably Kim et al. (2002), Malkawi et al. (2001), and Greco (1996).

Table 1.1 Material Properties

	c' (kN/m^2)	ϕ (deg.)	γ (kN/m^3)
Upper Layer	29.4	12	18.82
Middle Layer	9.8	5	18.82
Lower Layer	294.0	40	18.82

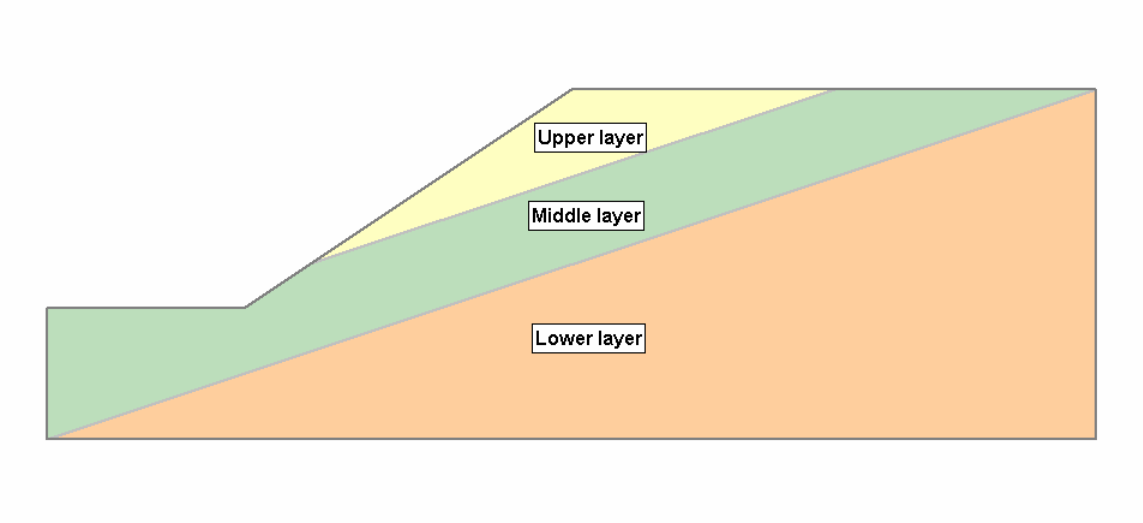

Figure 1.1 Slope geometry

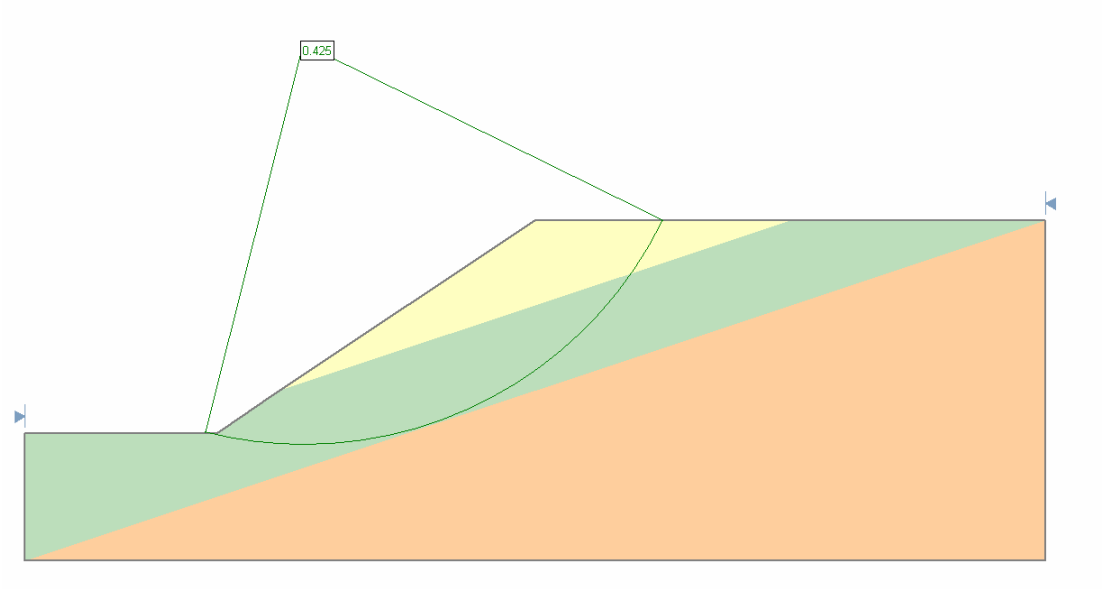

Figure 1.2 Circular Auto Refine Search Method, Spencer Method (FOS: 0.425)

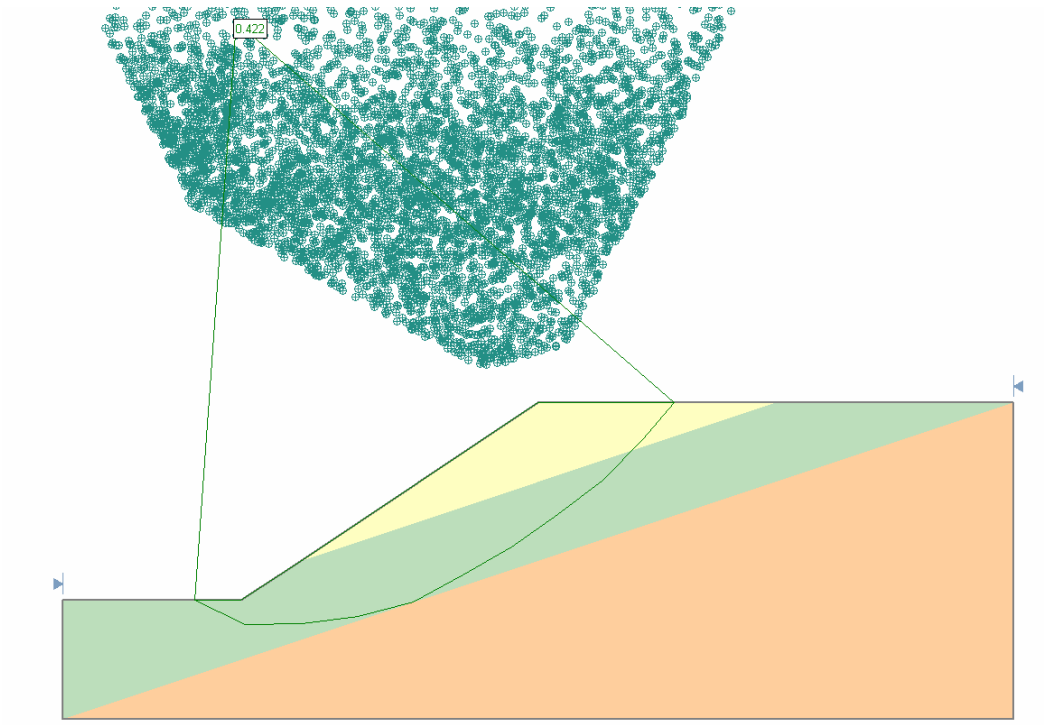

Figure 1.3 Non-Circular Path Search Method, Spencer Method (FOS: 0.422)

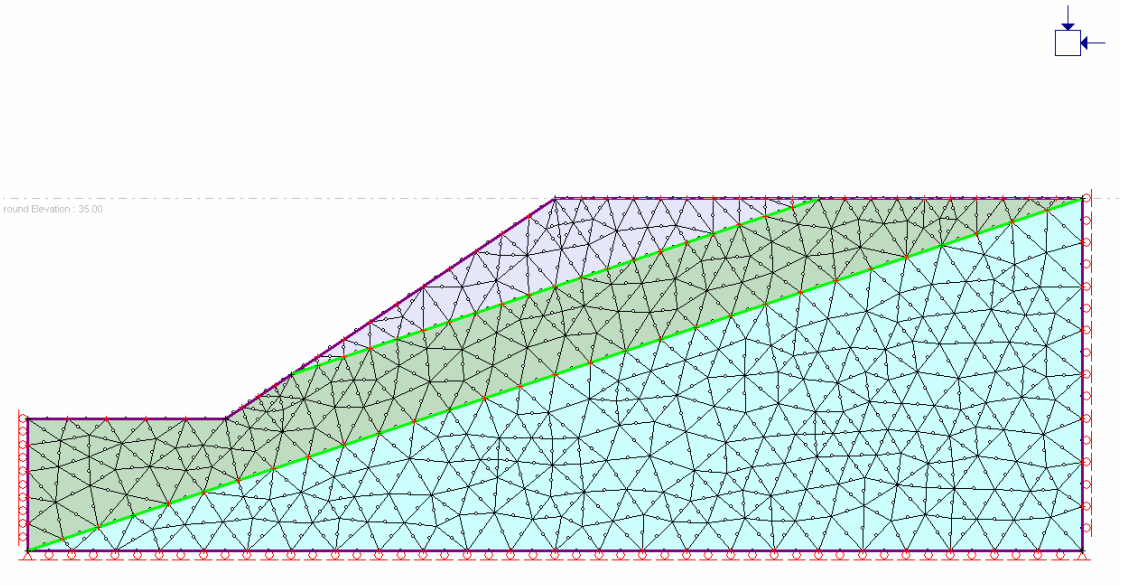

Figure 1.4 Phase^2 Finite Element Mesh (6-Noded triangles)

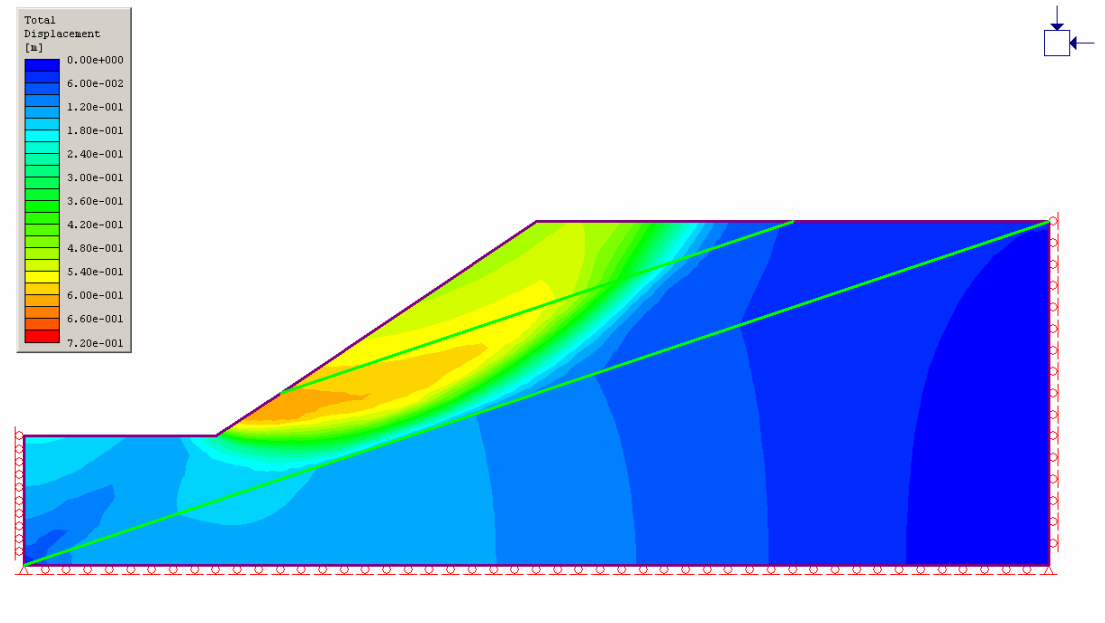

Figure 1.5 Total Displacements Contours
(SRF = 0.39)

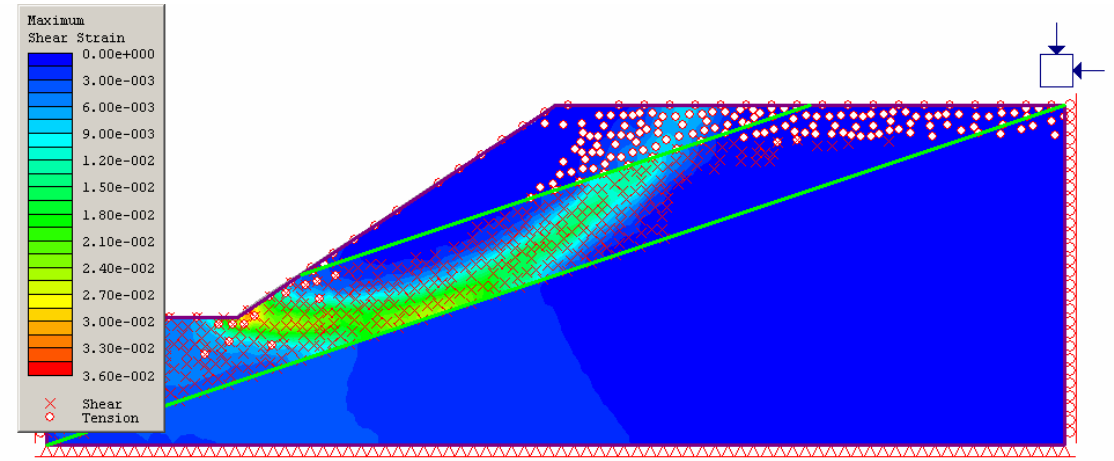

Figure 1.6 Maximum Shear Strain Contours and shear yielded elements (SRF = 0.39)

Table 1.2 Strength Reduction Factor

Strength Reduction Factor	Maximum Total Displacement (m)
0.35	0.0668
0.375	0.0715
0.39	0.0783
0.40	0.1750

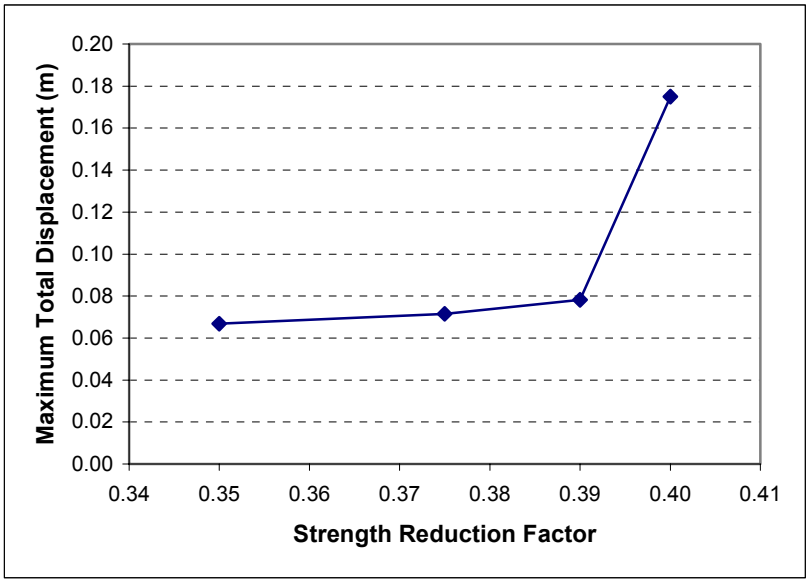

Figure 1.7 Strength reduction factor plotted against the maximum total displacement

Table 1.2 Factor of Safety

Method	Failure Surface	Factor of Safety
Limit Equilibrium Method	Circular	0.425
	Non-Circular	0.422
Finite Element Method		0.390

II. Example 2 (Slide verification example #19)

This model is taken from Greco (1996) example #4 and was originally published by Yamagami and Ueta (1988). It consists of a layered slope without pore pressure. The material properties are given in Table 2.1. The position of the critical slip surface and the corresponding factor of safety are calculated for a noncircular slip surface.

Table 19.1: Material Properties

	c' (kN/m^2)	ϕ (deg.)	γ (kN/m^3)
Upper Layer	49	29	20.38
Layer 2	0	30	17.64
Layer 3	7.84	20	20.38
Bottom Layer	0	30	17.64

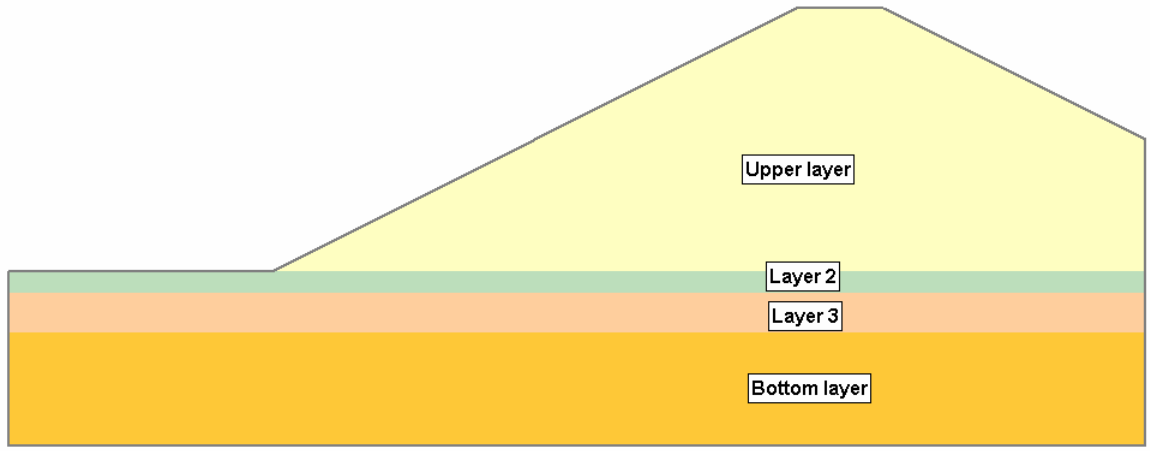

Figure 2.1 Slope geometry

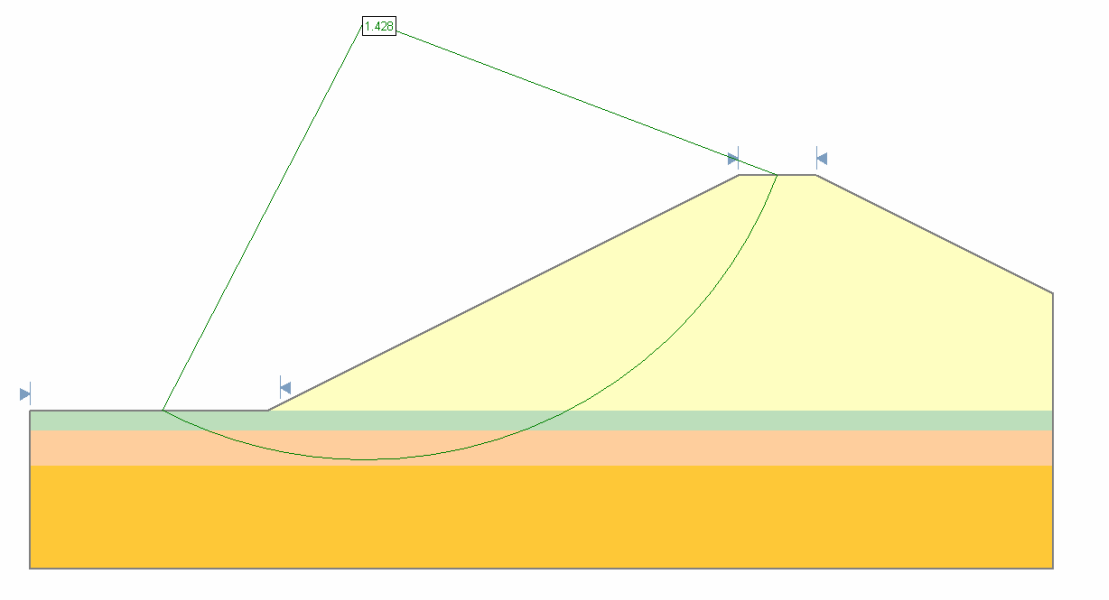

Figure 2.2 Circular Auto Refine Search Method, Spencer Method (FOS: 1.428)

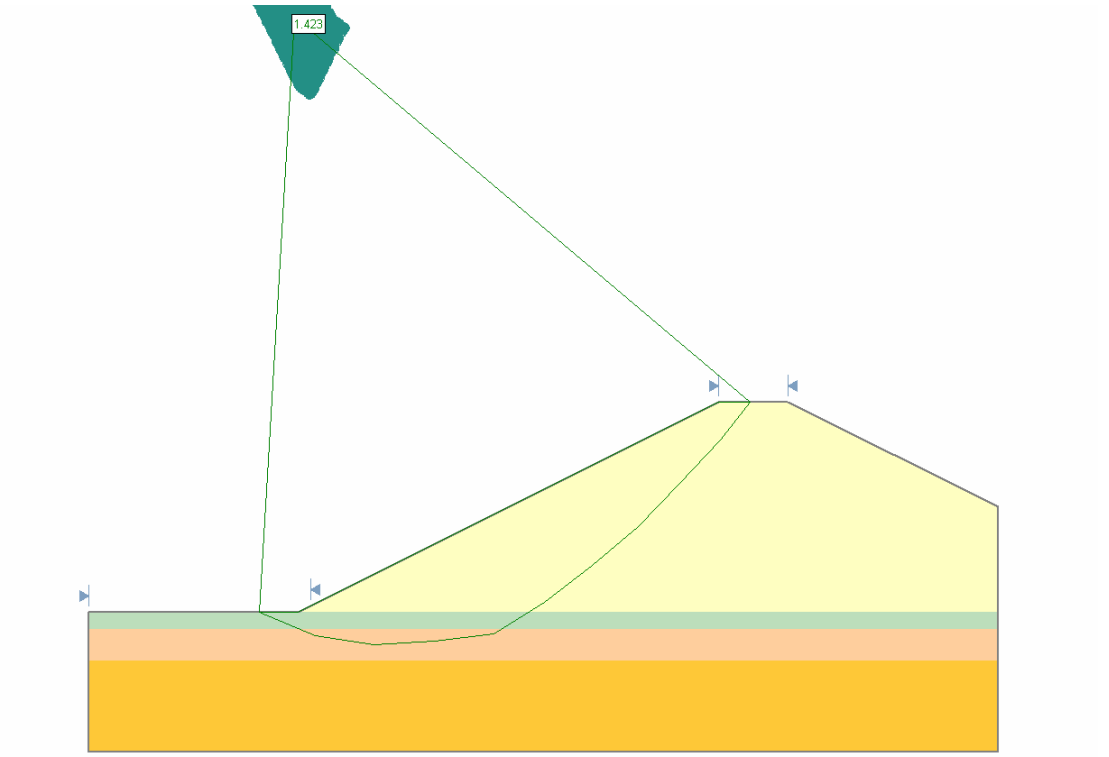

Figure 2.3 Non-Circular Path Search Method, Spencer Method (FOS: 1.423)

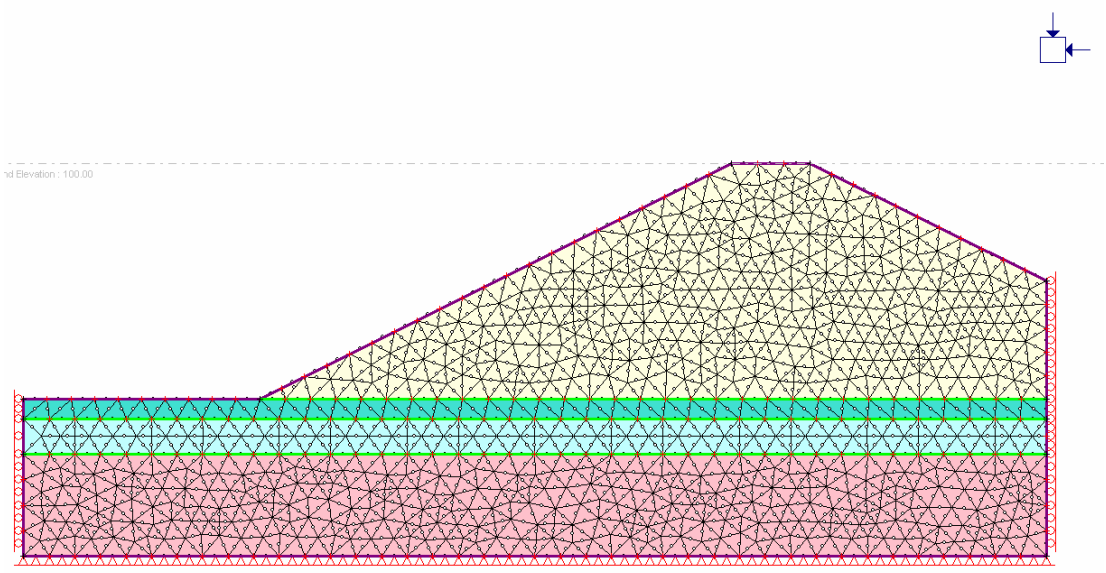

Figure 2.4 Phase^2 Finite Element Mesh (6-Noded triangles)

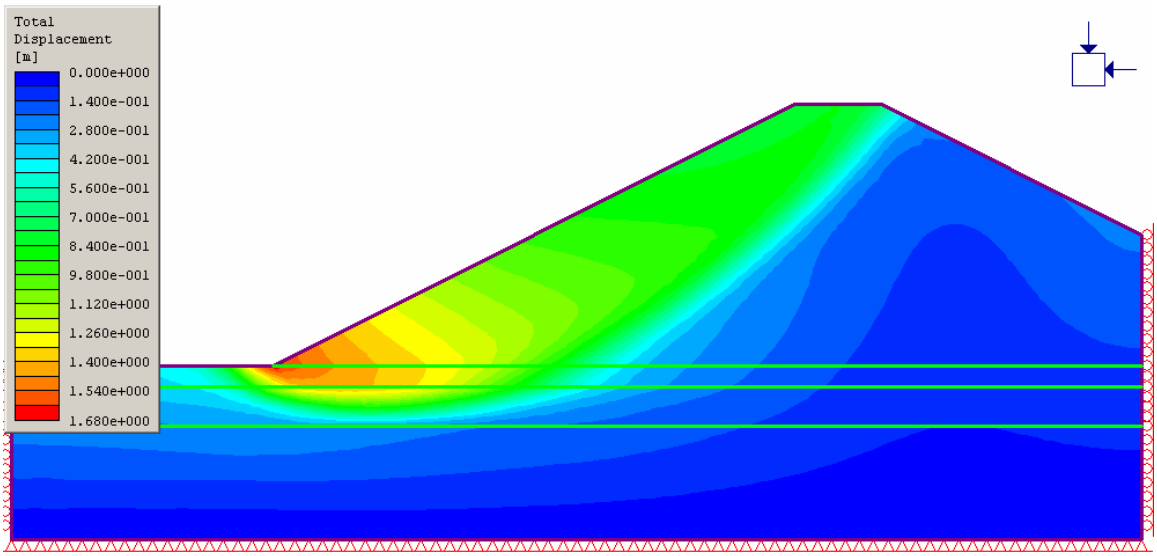

Figure 2.5 Total Displacements Contours (SRF = 1.4)

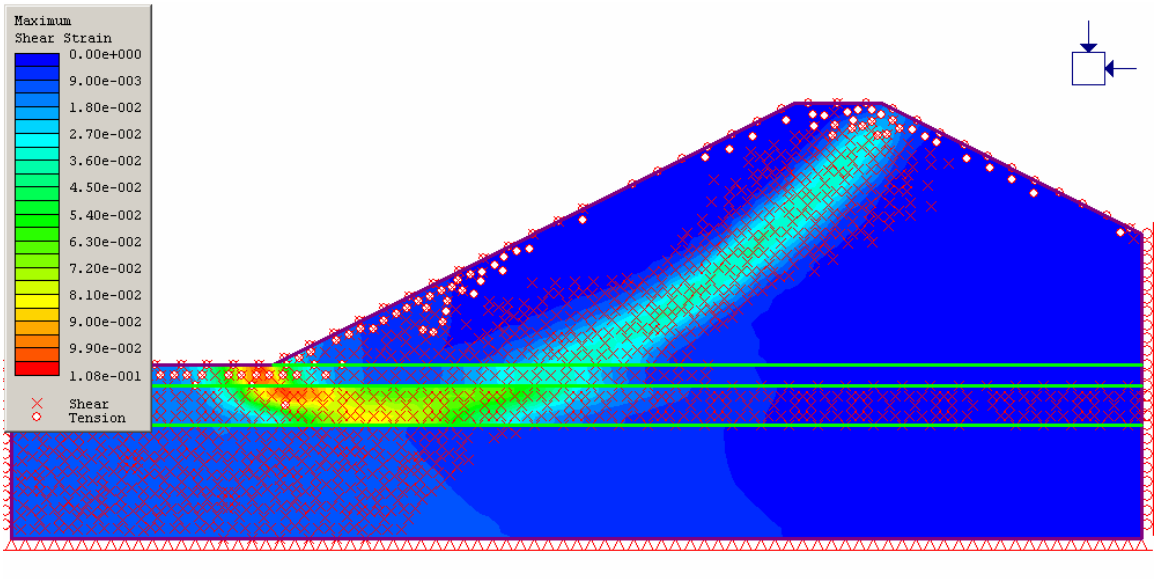

Figure 2.6 Maximum Shear Strain Contours and shear yielded elements (SRF = 1.4)

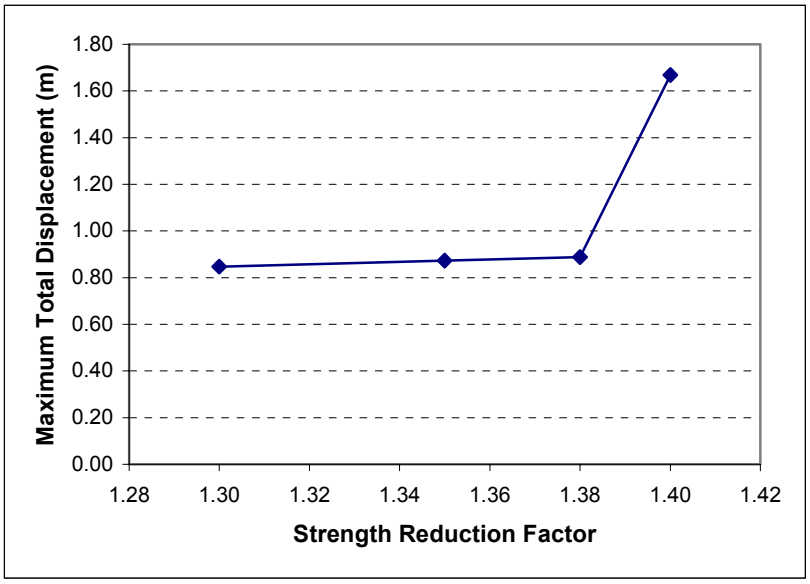

Figure 2.7 Strength reduction factor plotted against the maximum total displacement

Table 2.2 Factor of Safety

Method	Failure Surface	Factor of Safety
Limit Equilibrium Method	Circular	1.428
	Non-Circular	1.423
Finite Element Method		1.38

III. Example 3

This model is taken from Kockar and Akgun (2003) example 1. The slope stability analysis was performed at the side/cut slope sections. Circular and non-circular failure analogies were used for the slope stability analyses of irregularly jointed, highly foliated lithologies.

Table 3.1 Material Properties

	c (kN/m^2)	ϕ (deg.)	γ (kN/m^3)
Rock	78	23	26.65

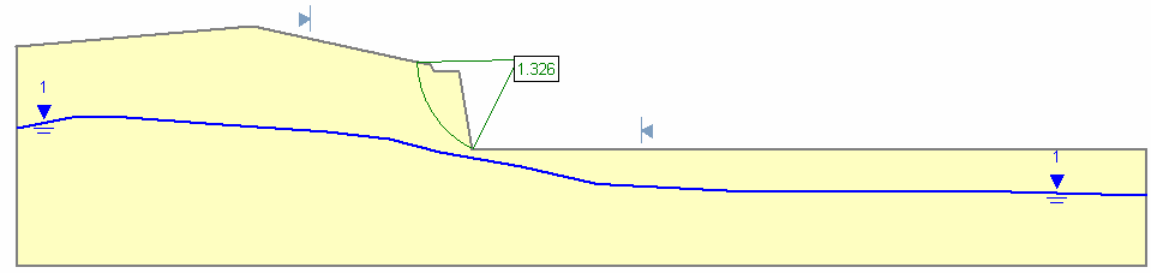

Figure 3.1 Circular Slope Search Method, Bishop's Method (FOS: 1.326)

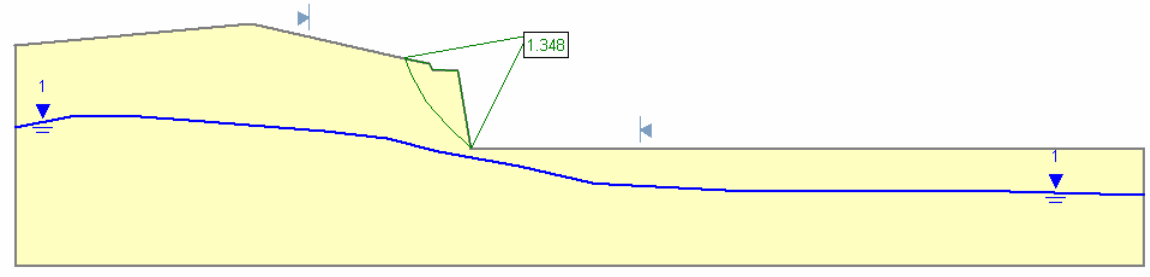

Figure 3.2 Non-Circular Path Search Method, Bishop's Method (FOS: 1.348)

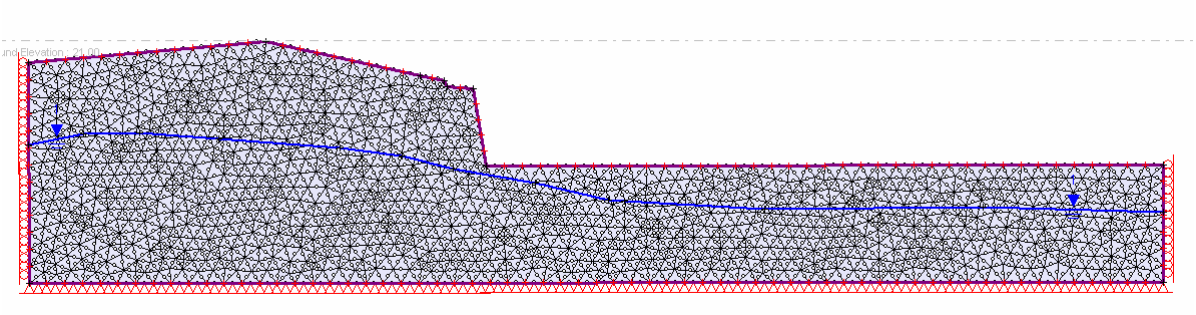

Figure 3.3 Phase^2 Finite Element Mesh (6-Noded triangles)

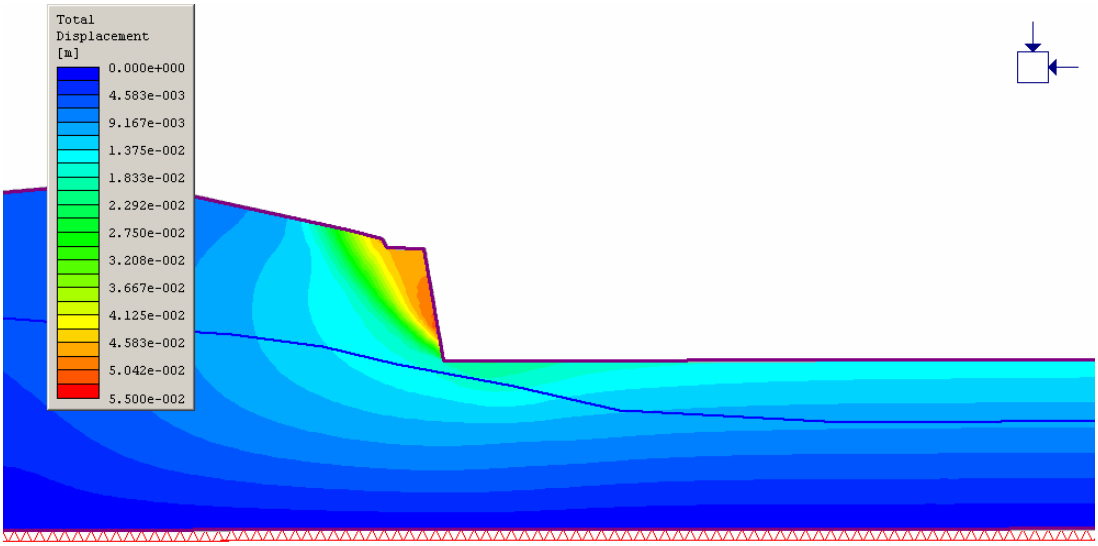

Figure 3.4 Total Displacements Contours
(SRF = 1.3)

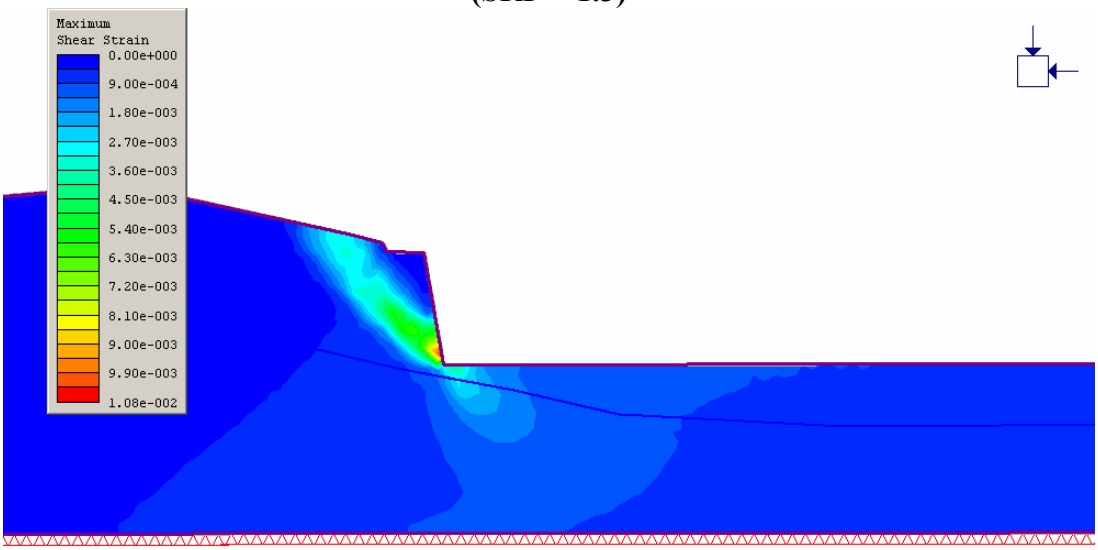

Figure 3.5 Maximum Shear Strain Contours
(SRF = 1.3)

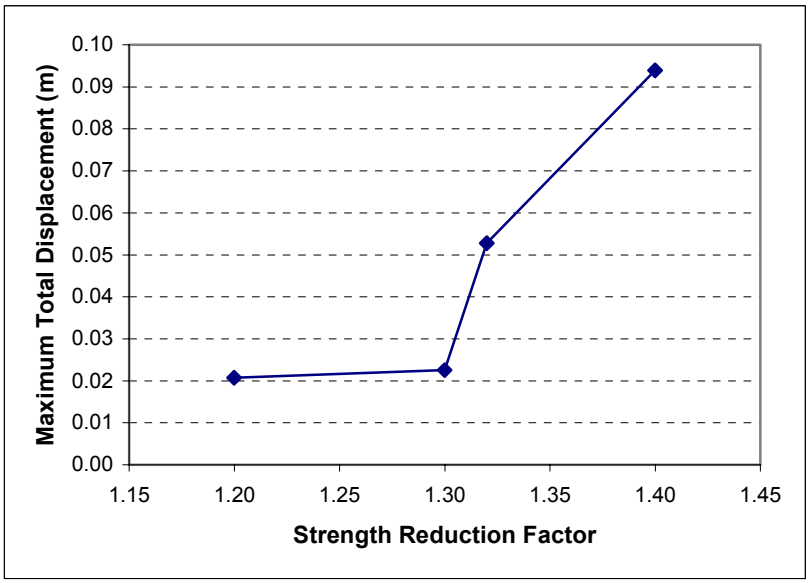

Figure 3.6 Strength reduction factor plotted against the maximum total displacement

Table 3.2 Factor of Safety

Method	Failure Surface	Factor of Safety
Limit Equilibrium Method	Circular	1.326
	Non-Circular	1.348
Finite Element Method		1.300

IV. Example 4

This model is taken from Kockar and Akgun (2003) example 2. The slope stability analysis was performed at the side/cut slope sections. Circular and non-circular failure analogies were used for the slope stability analyses of irregularly jointed, highly foliated lithologies.

Table 4.1 Material Properties

	c (kN/m^2)	ϕ (deg.)	γ (kN/m^3)
Rock	78	23	26.65

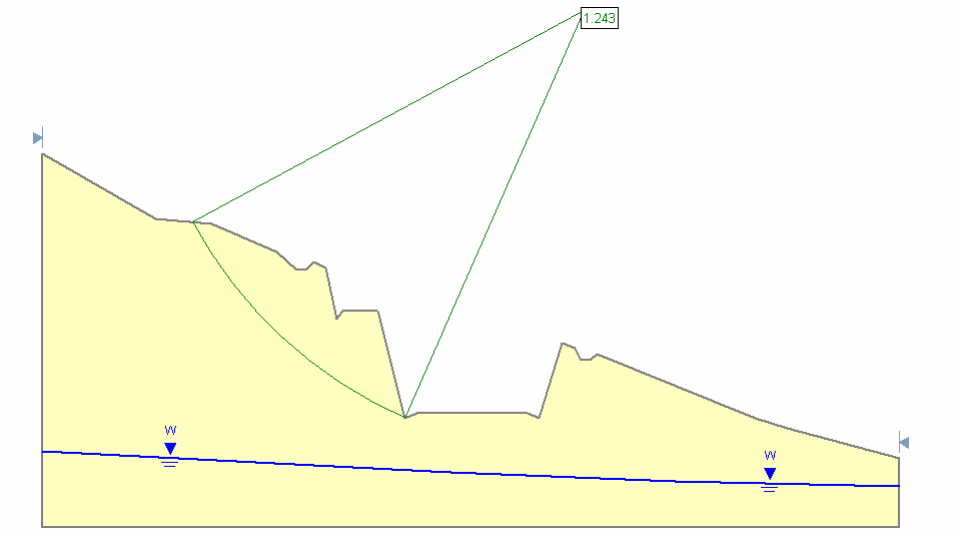

Figure 4.1 Circular Auto Refine Search Method, Bishop Method (FOS: 1.243)

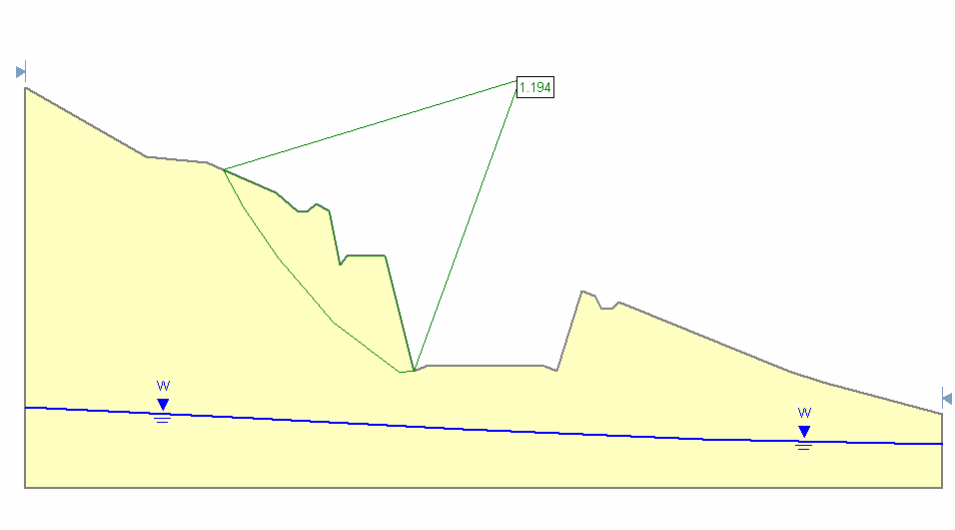

Figure 4.2 Non-Circular Path Search Method, Bishop Method (FOS: 1.19)

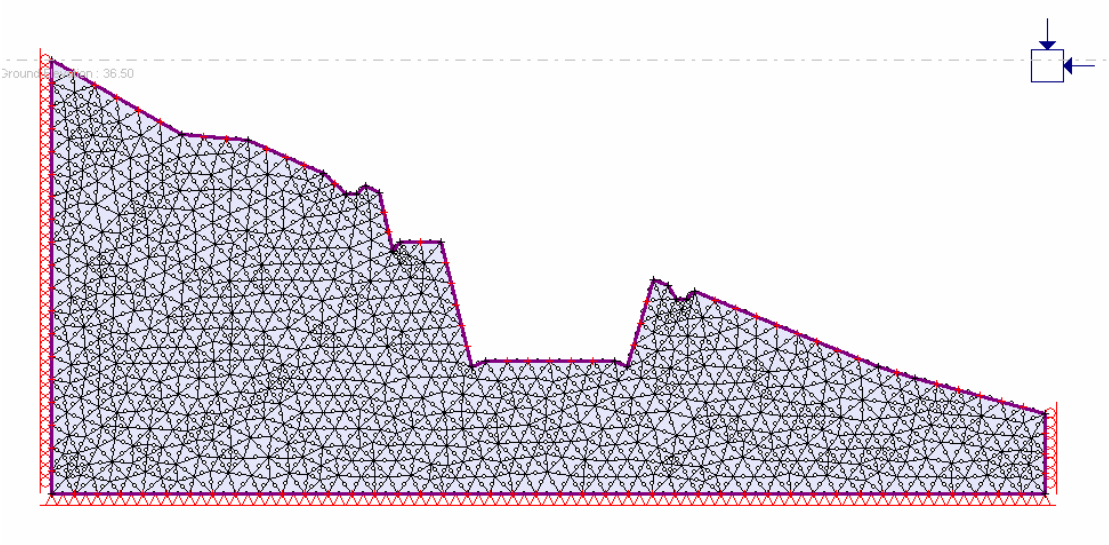

Figure 4.3 Phase^2 Finite Element Mesh (6-Noded triangles)

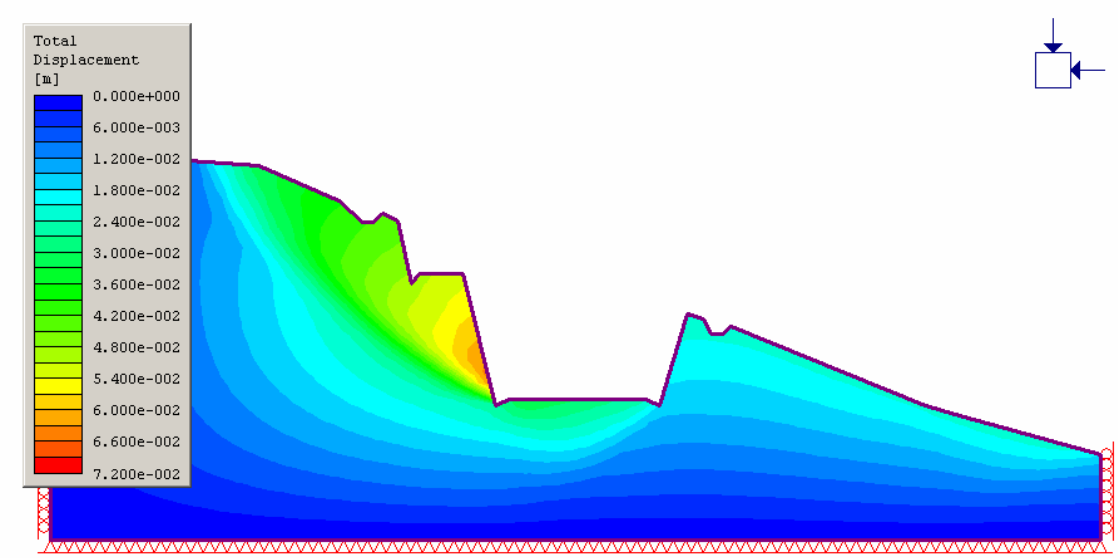

Figure 4.4 Total Displacements Contours
(SRF = 1.15)

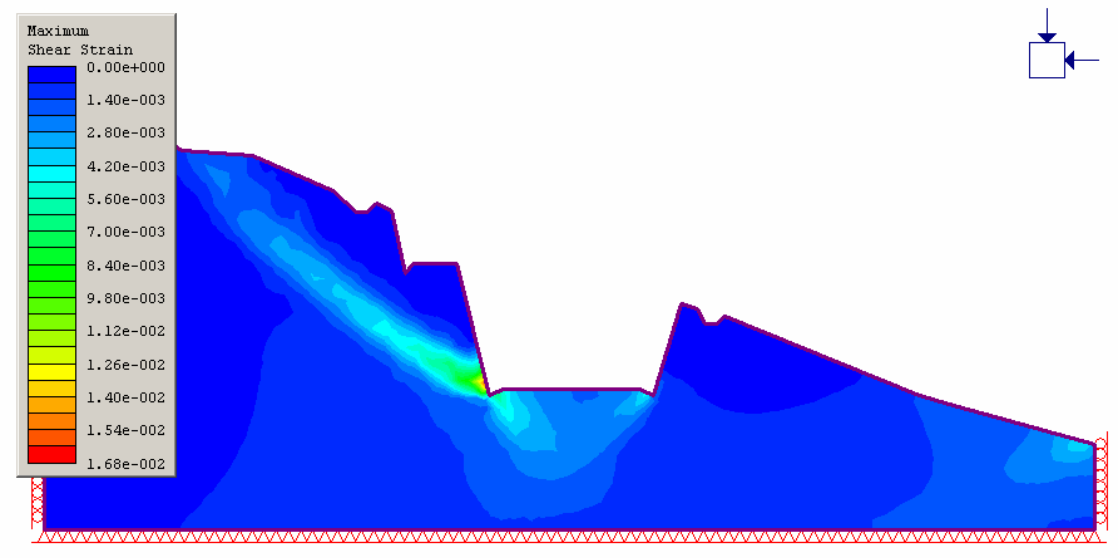

Figure 4.5 Maximum Shear Strain Contours
(SRF = 1.15)

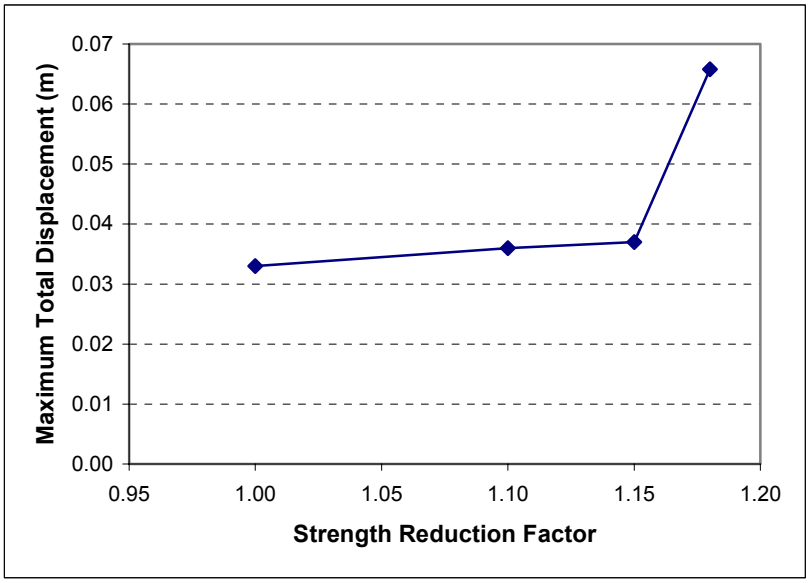

Figure 4.6 Strength reduction factor plotted against the maximum total displacement

Table 4.2 Factor of Safety

Method	Failure Surface	Factor of Safety
Limit Equilibrium Method	Circular	1.243
	Non-Circular	1.194
Finite Element Method		1.150

V. Example 5

This model is taken from Griffiths and Lane (1999) example 6. The example represents an actual earth dam including a free surface which slopes from the reservoir level to foundation level on the downstream side. Two cases studied in this example for empty reservoir and full reservoir.

Table 5.1 Material Properties

	c (kN/m^2)	ϕ (deg.)	γ (kN/m^3)
Rock	13.8	37	18.2

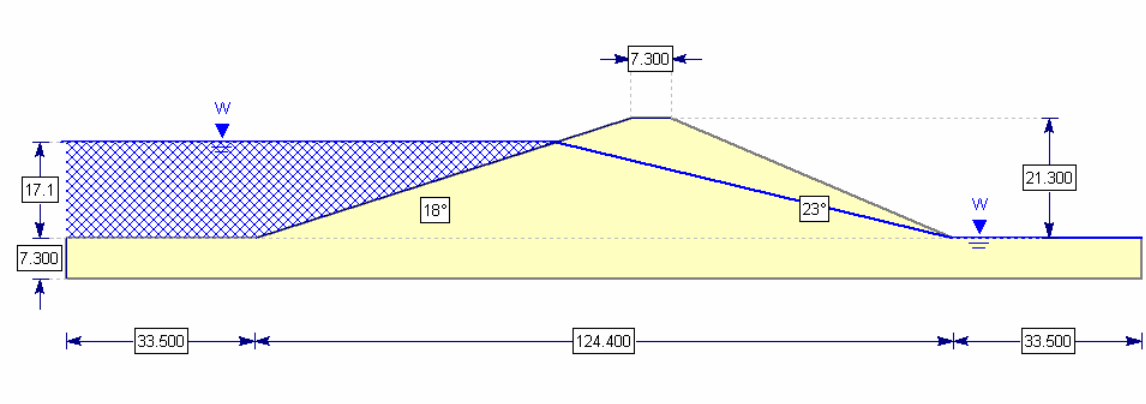

Figure 5.1 Slope geometry

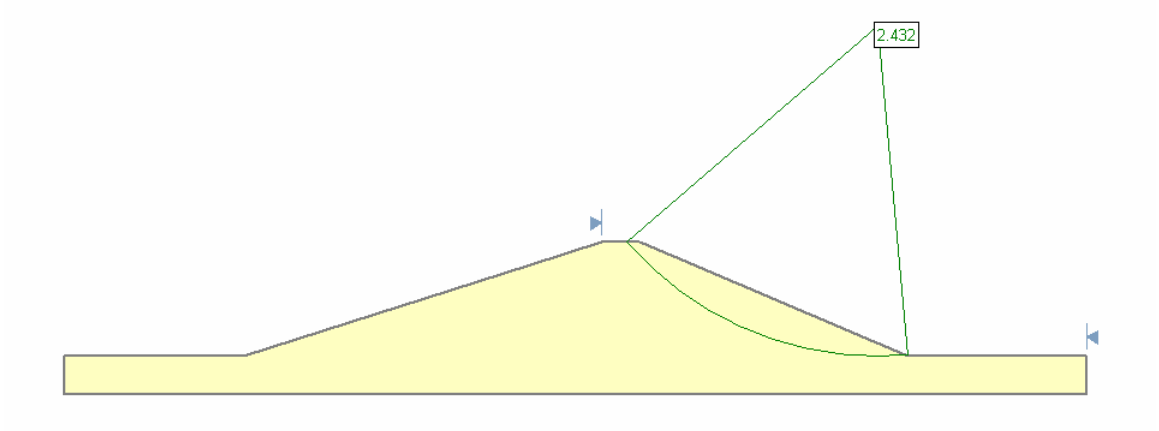

Figure 5.2 Circular Auto Refine Search Method, Bishop Method (FOS: 2.432)

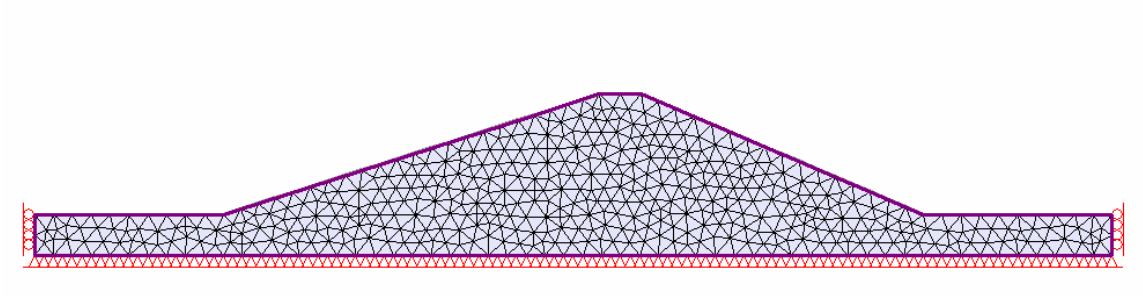

Figure 5.3 Phase^2 Finite Element Mesh (6-Noded triangles)

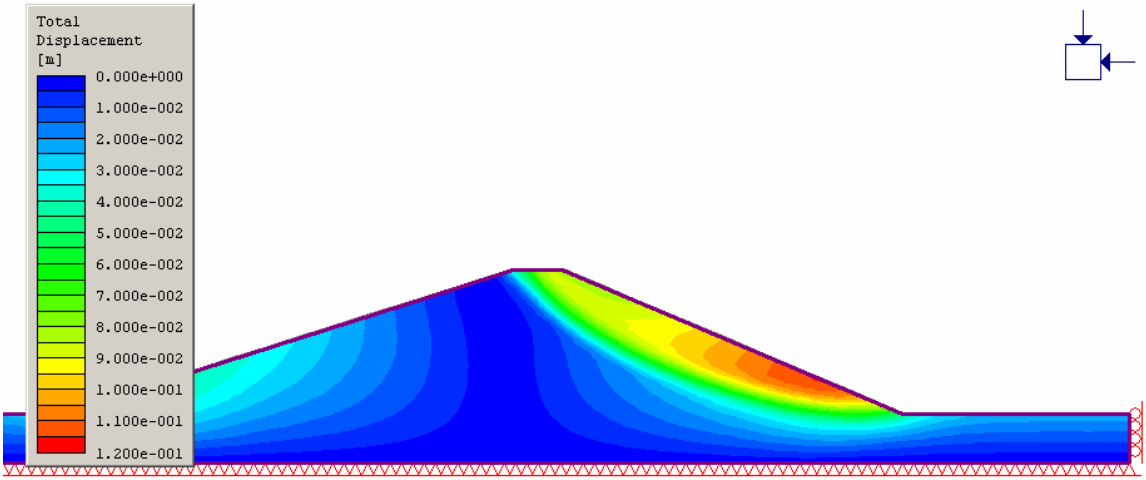

Figure 5.4 Total Displacements Contours
(SRF = 2.45)

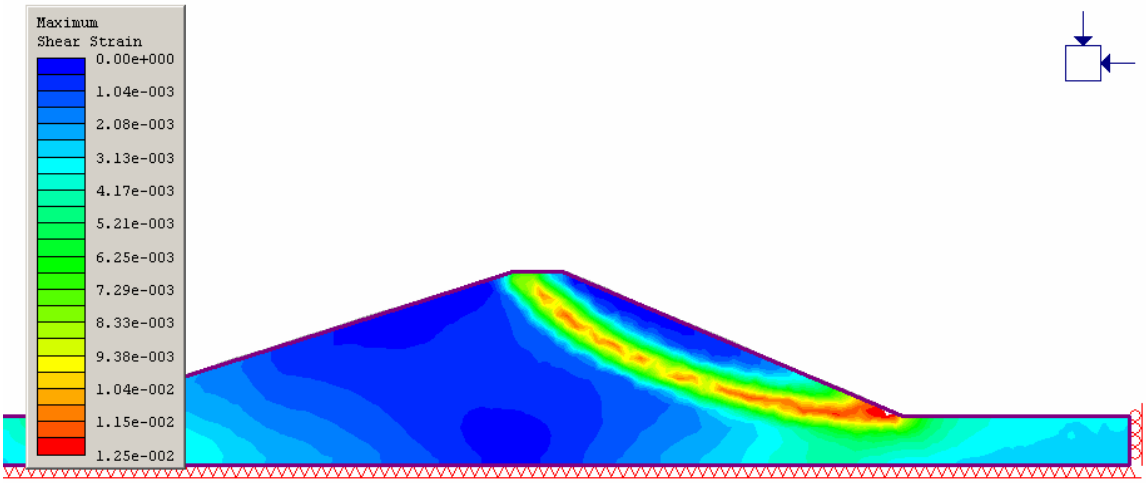

Figure 5.5 Maximum Shear Strain Contours
(SRF = 2.45)

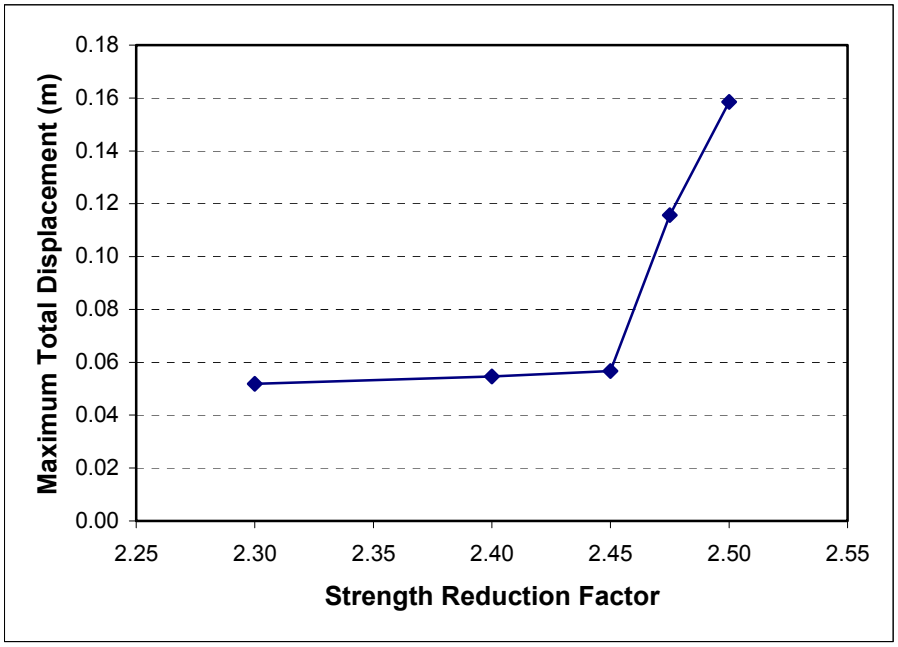

Figure 5.6 Strength reduction factor plotted against the maximum total displacement

Table 5.2 Factor of Safety

Method	Failure Surface	Factor of Safety
Limit Equilibrium Method	Circular	2.432
Finite Element Method		2.450

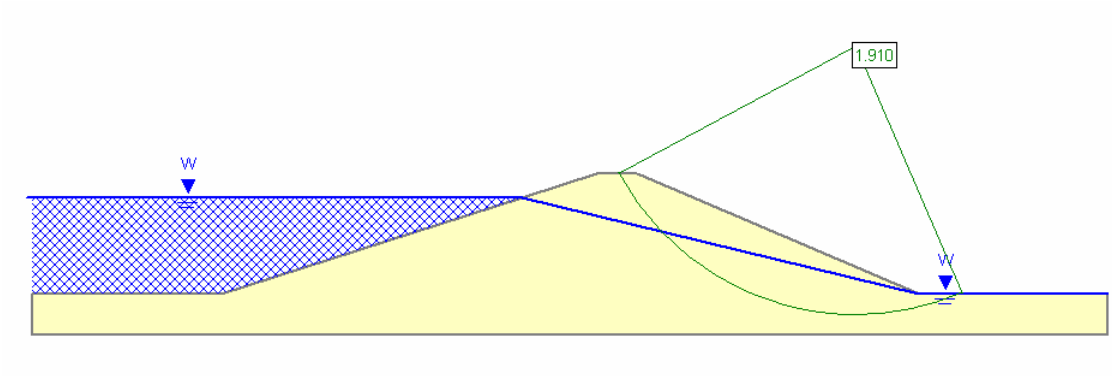

Figure 5.7 Circular Auto Refine Search Method, Bishop Method (FOS: 1.91)

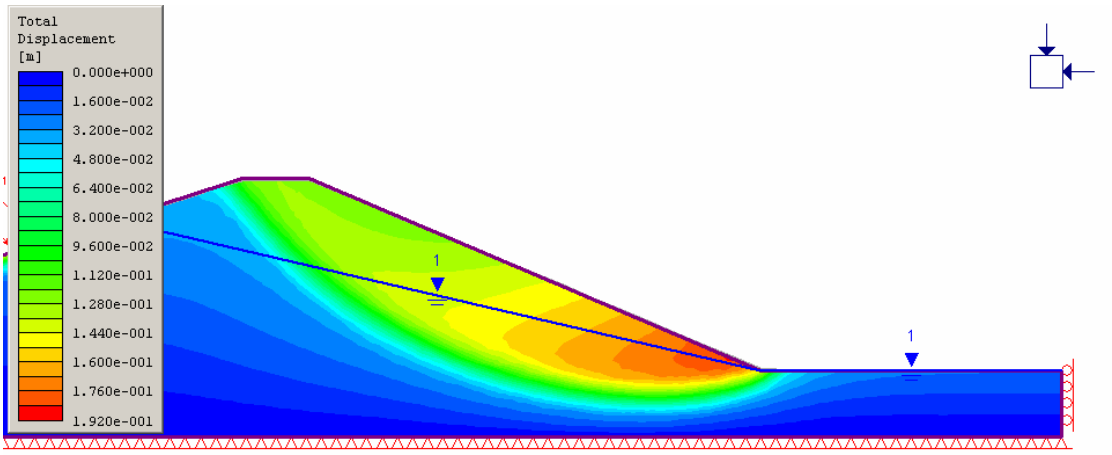

Figure 5.8 Total Displacements Contours (SRF = 1.85)

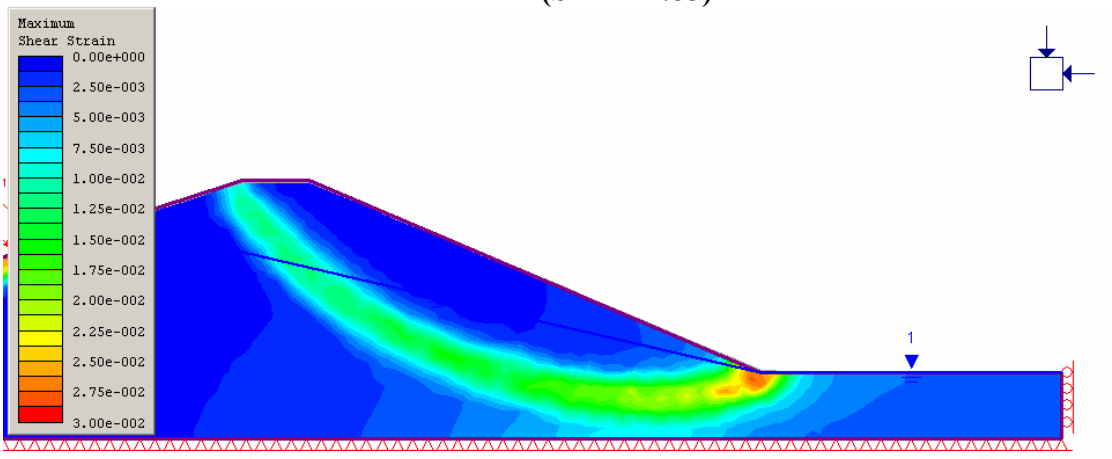

Figure 5.9 Maximum Shear Strain Contours (SRF = 1.85)

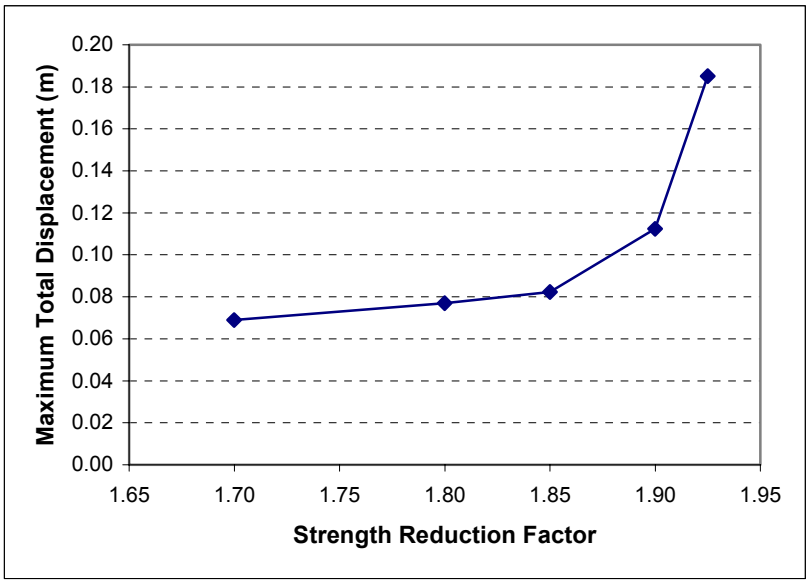

Figure 5.10 Strength reduction factor plotted against the maximum total displacement

Table 5.3 Factor of Safety

Method	Failure Surface	Factor of Safety
Limit Equilibrium Method	Circular	1.91
Finite Element Method		1.85

Reference:

1. Arai, K., and Tagyo, K. (1985), “Determination of noncircular slip surface giving the minimum factor of safety in slope stability analysis.” Soils and Foundations. Vol.25, No.1, pp.43-51.

2. Malkawi, A.I.H.,Hassan, W.F., and Sarma, S.K. (2001), “Global search method for locating general slip surfaces using monte carlo techniques.” Journal of Geotechnical and Geoenvironmental Engineering. Vol.127, No.8, August, pp. 688-698.

3. Greco, V.R. (1996), “Efficient Monte Carlo technique for locating critical slip surface.” Journal of Geotechnical Engineering. Vol.122, No.7, July, pp. 517-525.

4. Kim, J., Salgado, R., Lee, J. (2002), “Stability analysis of complex soil slopes using limit analysis.” Journal of Geotechnical and Geoenvironmental Engineering. Vol.128, No.7, July, pp. 546-557.

5. Yamagami, T. and Ueta, Y. (1988), “Search noncircular slip surfaces by the Morgenstern-Price method.” Proc. 6th Int. Conf. Numerical Methods in Geomechanics, pp. 1335-1340.

6. M.K. Kockar, H. Akgun (2003), “Methodology for tunnel and portal support design in mixed limestone, schist and phyllite conditions: a case study in Turkey.” Int. J. Rock Mech. and Min Sci, Vol. 40, pp. 173–196.

7. Griffiths, D. V. and P. A. Lane (1999), "Slope Stability analysis by finite elements." Geotechnique **49**(3): 387-403.